Shri Shamrao Patil (Yadravkar) Educational & Charitable Trust's

SHARAD INSTITUTE OF TECHNOLOGY, COLLEGE OF ENGINEERING

Yadrav (Ichalkaranji), Dist.-Kolhapur (Maharashtra)

▪ NBA Accredited Programmes ▪ NAAC 'A' Grade Institution ▪ An ISO 9001 : 2015 Certified Institute

AN AUTONOMOUS INSTITUTE

Tarang

Technical Magazine

AY 2022-23

DEPARTMENT OF ELECTRICAL ENGINEERING

Department Vision and Mission

VISION

To be a center of excellence in Electrical Engineering education to prepare professionally competent engineers with lifelong learning attitude for the accomplishment of ever-growing needs of society.

MISSION

- To prepare technically and professionally competent engineers by imparting quality education through effective teaching learning methodologies and providing stimulating environment for research and innovation.
- To develop professional skills and right attitude in students that will help them to succeed and progress in their personal and professional career.
- To imbibe moral and ethical values in students with concern to society and environment.

Program Educational Objectives (PEOs)

Graduates of the program will

- PEO I : Engage in design of system, tools & application in the field of electrical engineering & allied engineering industries.
- PEO II : Apply the knowledge of electrical engineering to solve problems of social relevance, pursue higher education & research.
- PEO III: Engage in lifelong learning, career enhancement & adapt to changing professional & societal needs.

Program Specific Outcomes (PSOs)

- PSO 1 : Identify, formulate and analyse electrical engineering problems for real life industrial and societal needs.
- PSO 2 : Design and develop systems in the emerging electrical engineering and allied disciplines to meet out the industry standards.

EXECUTIVE DIRECTOR‛S MESSAGE:

Good things remain good only because they are always scant. I am glad to unfold this wonderful magazine as an appreciation of the admirable efforts put forth by the team. The effort taken to bring about content is appreciable. This is a productive technical material and subsidiary skill developing tool for the students. The release of this brilliant forth issue of the technical magazine “TARANG” has added the value of department. Ialso applaud the coordination & efforts behind the team to bring out this issue.

Hon.Shri Anil A Bagane
Executive Director
Sharad Institute of Technology
College of Engineering, Yadrav

PRINCIPAL’S MESSAGE:

We have been gifted with this blessed life. The program of society is mainly depend on many people who are working behind the scenes ,overtime round the clock planning things to the smallest. This technical magazine will be a medium to provide proper acknowledgement and respect to all of these effort and its results. This is only small step towards a long journey. This fourth issue of technical magazine should inspire all of us for a new beginning enlighten with hope , confidence and faith in each other In the road ahead for innovation work. It is expected that wide support for this mission will be provided through the reader’s valuable suggestions and comments…….Happy reading.

Dr. Sanjay A Khot
Principal
Sharad Institute of Technology
College of Engineering, Yadrav

HOD'S MESSAGE:

Ifeel delight to introduced Seventh Issue of Technical Magazine prepared by department of Electrical Engineering. We at SITCOE promise of increasing the knowledge, enhancing the critical thinking, ability to change information into knowledge & power of analyzing the things technically of each & every individual of ever changing society through students.

Dr.K Hussain
Head of the Department

FACULTY EDITOR MESSAGE:

Greetings from the Editorial members board of the Technical Magazine "TARANG Volume VII". It is the snap shot of the various technologies and technological changes associated with Electrical Engineering.

We profusely thank our Honorable Executive Director Shri Anil Bagane, Principal Dr. Sanjay A Khot and Head of Electrical Engineering Department Dr. K Hussain for giving support and encouragement and a free hand in this endeavor. This Technical Magazine will be a medium to provide proper acknowledgement and respect to all of those efforts and its results.

Wishing you Happy Reading

Mr. Chandrashekhar Patil
Assistant Professor
Dept.of Electrical
Engineering

Third Year Electrical Engineering

It’s truly an interesting and exciting experience for all of us as student editors of this technical magazine “TARANG Volume VII for was one such cherished work that had its roots in the persuasion. It would be a snap shot of the various activities and advancements in the field of Electrical Engineering Dept.

This Technical Magazine will serve to reinforce and allow increased awareness about research activities. Interaction and Team Work among all of us, usually we fail to appreciate the good deeds of many people and activities that happen around us as we are engaged in irrelevant talks and assumptions. It could all change if we just pause to think of what is our contribution to the society.

Miss Simran Tabarej Hukkeri

Miss Tejaswinee Rangrao Kadam

Miss Ashwini Parshuram Ghavale

Index

The Artificial Leaf

Name: Miss.Simran Tabarej Hukkeri.

Class: TY Electrical Engineering

Abstract:

To convert the energy of sunlight into chemical energy, the leaf splits water via the photosynthetic process to produce molecular oxygen and hydrogen, which is in a form of separated protons and electrons. The primary steps of natural photosynthesis involve the absorption of sunlight and its conversion into spatially sepalratedelectronhole pairs. The holes of this wireless current are captured by the oxygen evolving complex (OEC) of photo system II (PSII) to oxidize water to oxygen. The electrons and protons produced as a byproduct of the OEC reaction are captured by ferrodoxin of photo system I. With the aid of ferrodoxin NADP+reeducates, they are used to produce hydrogen in the form of NADPH. For a synthetic material to realize the solar energy conversion function of the leaf, the light-absorbing material must capture a solar photon to generate a wireless current that is harnessed by catalysts, which drive the four electron/hole fuel-forming water-splitting reaction under benign conditions and under 1 sun (100 mW/cm2) illumination. To stabilize silicon in water, its surface is coated with a conducting metal oxide onto which the Co-OEC may be deposited. The net result is that immersing a triple-junction Si wafer coated with NiMoZn and Co-OEC in water and holding it up to sunlight can effect direct solar energy conversion via water splitting. By constructing a simple, stand-alone device composed of earth-abundant materials, the artificial leaf provides a means for an inexpensive and highly distributed solar-to-fuels system that employs low-cost systems engineering and

manufacturing. Through this type of system, solar energy can become a viable energy supply to those in the non-legacy world.

Introduction:

An artificial leaf, silicon-based device that usesolar energy to split hydrogen and oxygen in water, thereby producing hydrogen energy in a clean way, leaving virtually no pollutants. The technology, which was designed to simulate the natural energy-generating process of photosynthesis used by plants, was first successfully developed by American chemist Daniel G. Nocera and colleagues in 2011. Further work was needed to improve its efficiency and cost-effectiveness for practical use.

Figure 1: Artificial Leaf

The basic component of an artificial leaf is a silicon chip that is coated in chemical catalysts, which speed up the water-splitting reaction. In an open vessel of water, when solar energy hits the chip, a chemical reaction similar to photosynthesis occurs—the hydrogen and oxygen molecules of water are split apart, resulting in the separation of protons and electrons. The protons and electrons are captured on the chip and are recombined to form hydrogen gas, which can be used for immediate generation of electricity or stored for later use.

The primary application of the artificial leaf is the clean production of hydrogen, which is considered an alternative form of energy. Other means of capturing hydrogen fuel include steam reforming, in which high-temperature steam is reacted with methane in the presence of a metal catalyst, and hydraulic fracturing (or “fracking”), in which fluids containing chemicals are injected into the ground at high pressure in order to release natural gases (including hydrogen) from underground rock formations. Neither of those approaches is considered to be a “clean” form of hydrogen production, since both involve the release of potentially harmful chemicals into the environment.

The artificial leaf also makes hydrogen a renewable energy source, since sunlight and water are abundant on Earth. Hence, with the artificial leaf, individuals can locally produce their own energy and can live apart from an electricity grid. This offers a significant advantage in that hydrogen energy could be produced almost continuously anywhere and at any time. Based on Nocera’s initial design, with artificial leaf technology, an estimated one to three bottles of water could produce enough energy to power a single household in less-developed regions of the world.

Methodology:

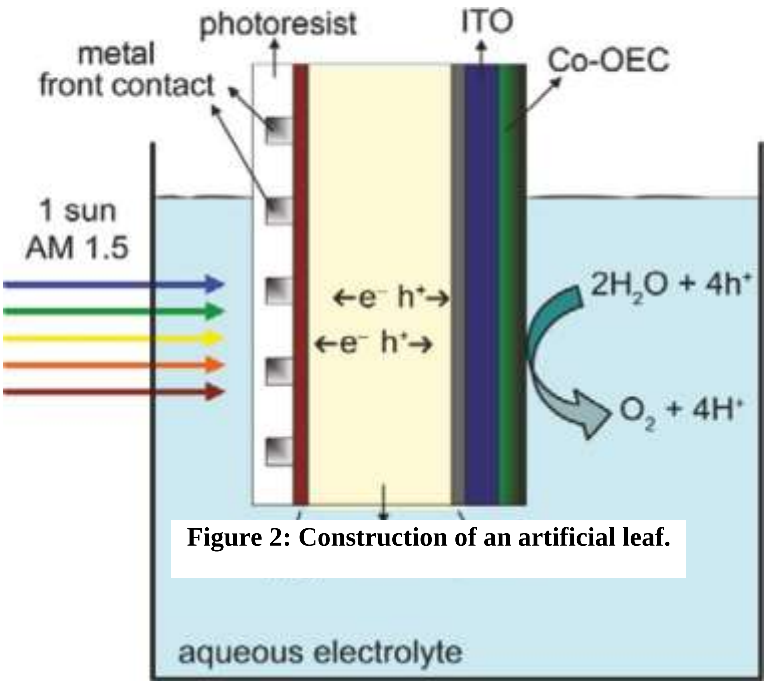

Figure 2: Construction of an artificial leaf.

The ability to perform water splitting with Co-OEC and NiMoZn catalysts in natural waters, under ambient conditions, and at high and stable current densities provides a direct path to the creation of an artificial leaf. The function of the photosynthetic membrane to capture solar light and convert it into a wireless current is assumed by Si. The photogenerated single electron and hole are relayed to the Co-OEC and NiMoZn catalysts, until the necessary four electron hole equivalents are attained to drive the bond rearrangement of water splitting.

Single Junction PEC Cell:

The first step to realizing the artificial leaf of Figure 10 is to integrate the Co-OEC with Si. This objective was established by constructing the single junction npp+ cell. The p+ was incorporated on the p-side of the junction by depositing a 1 µm film of silicon-doped (1%) Al, followed by rapid thermal annealing in N2 at 900C. The npp+ Si single junction displays improved performance because the space charge region in the p+ layer is thin enough to act as a tunneling layer. A metal front contact was deposited on the n-side of the sample to enable PEC measurements and was protected from the solution using a 10 µm layer of photo resist. The Si was protected from oxidation by sputtering on the p+-side of the junction a 50 nm film of ITO, which served as an Ohmic contact for hole transport from the uried Si junction.

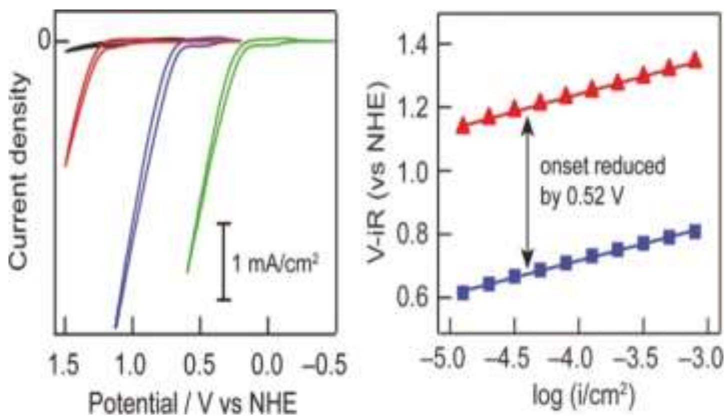

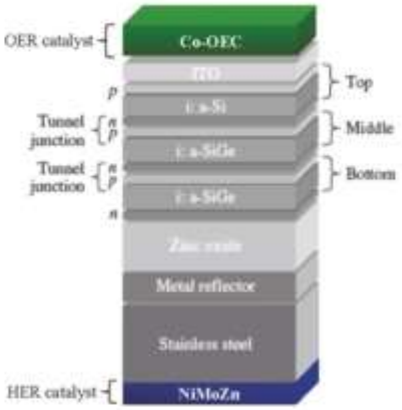

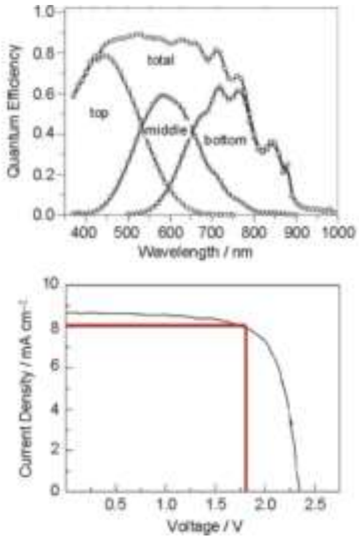

Figure 3 : Layers of Cell **Figure 4 : Graphical representation**

The Co-OEC catalyst maybe electrodeposited on the ITO barrier layer; alternatively the Co-OEC film may be also be grown from thin films of Co on a Si surface. Under these conditions, the thermodynamic potential for water oxidation is 0.82 V relative to the formal normal hydrogen electrode (NHE).

When the potential is applied through the ITO thin film in the dark (black trace in Figure 12), currentvoltage characteristics are the same as that of CoOEC on ITO or FTO electrodes. However, when the structure is illuminated from the n-side with 1 sun (100 mW/cm2) of AM 1.5 light, the potential onset for water oxidation decreases significantly. The onset of the cell under illumination requires 0.52 V less applied potential to induce water splitting at a given current density. Noting that this single junction cell generates 0.57 V, the majority of the photovoltage generated by the solar cell is utilized to drive the water splitting reaction. When an additional npp+ Si solar cell was connected in series to npp+ Si|ITO|Co-OEC and both cells were subjected to 1 sun illumination, the onset of the external applied potential is reduced by another 0.5. With these results in hand, we reasoned that the addition of a third Si solar cell would provide sufficient potential such that an external potential may be eliminated. Moreover, in seeking to create an artificial leaf, we imposed the further design guidelines of (i) no wiring, (ii) operation of the cell from water under simple conditions, and (iii) performing water splitting under 1 sun illumination.

Triple Junction Wireless Cell:

The Artificial Leaf. An artificial leaf comprising earth-abundant materials and that operates under simple conditions and at 1 sun has been realized by interfacing Co-OEC and NiMoZn with a triple junction amorphous Si (3jn-a-Si) solar cell.42 Stand-alone operation of the cell was achieved with the architecture shown in Figure 13. The 3jn-a-Si produces 8 mA cm2 of current at 1.8 V at an overall efficiency of 6.2%. As in the single junction cell, the p-side of the cell was protected with an ITO (or FTO) layer, on which the Co-OEC was electrodeposited. The NiMoZn HER alloy was electrodeposited onto the stainless steel support of the 3jn-a-Si cell. The stainless steel is not needed for the operation of the cell; it is present only as a structural support. The NiMoZn HER alloy may be deposited directly onto Si, and the HER is preserved. When the wireless CoPi |3jn-a-Si|NiMoZn wafer is immersed in an open container of electrolyte (1 M potassium borate, pH 9.2) and illuminated with 1 sun, O2 bubbles evolve from the anode at the front face and bubbles of H2 evolve from the cathode at the back of the wireless cell at an efficiency of 2.5%. Owing to the low solubility of O2 and H2 in water, the solar-to-fuels conversion process may be driven in the absence of a membrane. Overall solar-to-fuels efficiencies (SFE) were observed to be as high as 4.7% (for a 7.7% solar cell) when Ohmic losses are minimized. Noting that the overall solar-to-fuels efficiency is a product of the overall efficiency for water splitting and solar cell efficiency SFE(%) ¼ j(PV) 3 j(WS) (4) j(WS) is as high as 60%. This value compares well with cell efficiencies based on 3jn-a-Si PVs in which the a-Si is isolated from the electrolyte (SFE = 6% for j(PV) = 10%)4850 and for higher-efficiency systems using expensive PV materials (SFE = 18% for j(PV) = 28%).4852 Based on j(WS), higher overall cell efficiencies (>10%) may be readily achieved through the use of more efficient PVs. Even further increases in SFE may be realized by implementing engineering designs that minimize Ohmic resistances arising from ion transport.

Future Scope: Significant challenges remain, however, for artificial leaf technology. For example, more work is needed to improve efficiency; in initial studies, the artificial leaf captured only 4.7 percent of the total possible hydrogen fuel available in solar energy. Devices developed since then have achieved higher efficiencies (e.g., about 10 percent). Artificial leaf technology also remains potentially expensive, however, and concerns about the safety of hydrogen fuel storage limit practical implementation of the technology.

Conclusion: The artificial leaf achieves direct solar-to-fuels conversion at 1 sun (AM 1.5, 100 mA cm2) under benign conditions, using earth-abundant materials, and without the use of wires. The artificial leaf mimics nature inasmuch as it stores solar energy in water splitting by conforming to the functional elements of a leaf. We note that the actual leaf does not use hydrogen but stores it as a solid fuel, for example, carbohydrate. In the case of the artificial leaf, the hydrogen is available for combination with CO_2 as new catalysts for this process are discovered.

References:

[1]The Artificial Leaf DANIEL G. NOCERA* Department of Chemistry, 6-335, Massachusetts Institute of Technology, 77 Massachusetts Avenue, Cambridge, Massachusetts 02139-4307, United States RECEIVED ON NOVEMBER 23, 2011 https://pubs.acs.org/doi/10.1021/ar2003013

[2]Theartificial leaf technology**https://www.britannica.com/technology/artificial-leaf**

Characterization of Optical Redistribution LossDeveloped for Co-Packaged Optics

Name :TejaswineeRangraoKadam.
Class: TY Electrical Engineering

Abstract :
We previously proposed a new package substrate called active opticalpackage (AOP) substrate to realize co-packaged optics. An optical redistribution technology on silicon photonics dies was developed to fabricate the AOP substrate.Itis composed of a polymer waveguide, with a mirror-based optical coupling between the polymer and silicon waveguides. The fabricated optical redistribution loss wascharacterized in this study. An average loss of approximately 4 dB and wavelengthdependent loss of 1 dB were observed for the wavelength range of 1460–1600 nm. It wasshown that the low wavelength-dependent optical redistribution was available owing tothe broadband characteristics of mirror-based optical coupling and polymer waveguide.

Index Terms: Co-packaged optics, micro mirror, optical redistribution, polymerwaveguide, silicon photonics.

INTRODUCTION

ATA movement in high-performance computer systems and large-scale data centers is a critical concern. Increasing the data rates of conventional electrical links leads to lowlatency tolerance, high power consumption, and poor signal integrity, particularly forlong-distance interconnects. Co-packaging technologies for optics chips (e.g., Si photonics)and high-performance large-scale integration (LSI) chips have attracted remarkableattention as they can considerably reduce the length of high-data-rate electrical links. Forexample,at OFC 2018, Rockley Photonics demonstrated a switch application specificintegration circuit (ASIC) wherein Si photonics chipswere co packaged and a dozen ribbonoptical fibercables were connected to its package. Such massively parallel opticalinput/output (I/O) connections are necessary for high-performance LSIs such as theupcoming high-capacity switch ASICs that are expected to have data transfer rates ofover 100 Tbps.

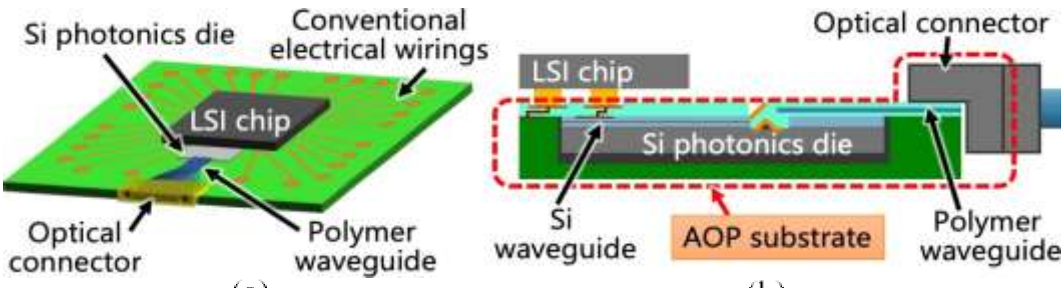

We previously proposed a new package substrate referred to as the active optical package(AOP) substrate, as a novel co-packaging solution. The bird's-eye view and cross-sectionalschematic of the AOP substrate are shown in Fig 1. The AOP substrate is based onconventional organic package substrates such as glass epoxy. In the package substrate, Si photonics dies are embedded as optical/electrical conversion devices. The electrical I/Os ofthe Si photonics dies are connected via thin film metallization (electrical redistribution).

Itsoptical I/Osare connected to standard single-mode fibers (SMFs) via optical redistribution,which is composed of polymer waveguides and micro mirrors, as shown in Fig. 1. Theoptical coupling between the polymer waveguides and SMFs is established by the opticalconnector, which is passively assembled at the edge of the package substrate.Implementing the AOP substrate eliminates the need for an accurate flip-chip bondingprocess of the Si photonics dies and active alignment of the optical fibers to the Si photonicsdies. Instead, the Si photonics dies are embedded in the package substrate using a roughalignment process.

Recently, we presented a feasibility study of the AOP substrate and demonstrated opticalredistribution on an Si photonics die. The loss of the fabricated optical redistribution andits wavelength dependence was also reported.In this letter, additional measurement resultsof the polymer waveguide optical characteristics and mirror surface profiles are provided. Onthe basis of these findings, we present further detailedanalysis of the measurement resultsconcerning the optical redistribution.

COMPONENTS FOR OPTICAL REDISTRIBUTION

Two components are required to realize optical redistribute-tion. The first is an opticalwaveguide that can be integrated on the package substrate, and the second is a couplingstructure between the optical waveguide and embedded Si photonics die. These componentsshould have low dependency on the wave- length and polarization in the desired transmissionwavelengthrange.

A polymer waveguide can be used as the optical waveguide.It can be fabricated by a low-temperature process. Therefore,it is suitable for fabrication as part of back-end processes.We used sunconnect (Nissan Chemical Industries Ltd.),a polymer waveguide material,as the broadband waveguide material in the transmission wavelength range. As the polymerwaveguides were connected to standard SMFs, their mode- field diameters (MFDs) must becomparable to those of the SMFs.

(c)

To connect the polymer and Si waveguides, a coupling structure based on two micromirrors was used. It provided low wavelength and polarization-dependent optical couplingas compared with a grating coupler, which is a popular surface coupling device. Asshown in Fig. 1, the light fromthe Si waveguide is output by the bottom-side mirror tothetop side. Next, the light is reflected again by the top-side mirror to the polymerwaveguide. The size (i.e., width and height) of the mirrors should be larger than the spotsizeof the optical beam between the polymer and Si waveguidesfor appropriate reflection.

Because the MFD of the polymer waveguide was adjusted to that of the SMF, the spot-sizediameter of the beam should be at least 10 µm. Therefore,the mirror size should be largerthan 14 µm. The coupling ofthe Si and polymer waveguides also required the connection ofmode-mismatched MFDs. The MFD of the Si waveguidewas increased to approximately 3µm upon using a Si inversetaper waveguide (a spot size converter (SSC)) at the endregionof the Si waveguide. However, there was still a largeMFD mismatch. To match the MFDof the Si and polymerwaveguides, a curved concave mirror was used as the bottom-side

mirror. Owing to the curved surface, the beam waist diameter of the light can be convertedfrom 3 µm to 10 µm. Thermal and mechanical tolerances of the optical redistribution based

on the above-mentioned components should be considered for practical applications. In ourprevious work,sensitivity to thermal deformation was studied for the coupling structure andwe showed that the structure had a high thermal tolerance. Tolerance evaluation to thepackage warpage,especially to study a behavior of the embedded Si photonicsdies, is one of the future works. If the Si photonics die and the package substrate are bent inthe same way, the war page will not cause critical problem since the coupling structure is avery small local structure while the package war page is a very large globaldeformation. That is, the global war page will cause negligible deformation in the localcoupling structure. And the war page of the polymer waveguide will not cause considerablebending loss.

I. FABRICATION

The fabrication process of optical redistribution on the Si photonics die was reported indetail in the previous report. First, a cavity was formed on the surface of the Si photonicsdie to integrate a bottom-side mirror. Next, the mirror was fabricated by gray-scalelithography, as described previously. Then, the mirror was coated with a reflectivemetal layer and encapsulate by a transparent resin. Subsequently, a bottom cladding and coreof the polymer waveguide were fabricated. Finally, the top-side mirror and top cladding werefabricated via the same gray-scale lithography process.The polymer waveguides were fabricated to have an MFD, comparable to the standardSMF (10μm), by controlling its size and refractive index. A cross-sectional opticalmicroscopic image of the polymer waveguide is shown in Fig. 2(a). The core width andheight were 9.1 and 6.8 μm, respectively. The near-field pattern (NFP) and far-field pattern(FFP) are shown in Fig. 2(b). The NFP and FFP diameter were 7.8 μm and12.4◦, respectively, on average. Thus, the polymer waveguide had an MFD that wascompatible with standard SMFs. The measured insertion loss spectrum of the 25-mm longpolymer waveguide is shown in Fig2(c). As shown in the spectrum, the polymer waveguidehas transparent broadband characteristics in the S, C, and L band. A coupling loss of0.5 dB was estimated for the input and output facet. Therefore, the propagation losswas 1 dB/cm at a wavelength of 1550 nm. Micro mirrors with a width and height of 20 and14 μm, respectively, were fabricated using gray-scale lithography. Laser microscopic imagesand surface height profiles of thefabricated mirrors are shown in Fig. 3. The mirrors were sufficiently large to perfectly reflectthe light beam with an MFD of 10 μm. To examine the detailed mirror surfaces, the 45∘rotated profiles of the mirror surface are also shown in Fig. 3. Smooth mirror surfaces wereobtained for the bottom and top-side mirrors. However, the profiles were slightly tilted so thatthe mirror angles were approximately 46∘. There were some deformed areas in the mirrorsurfaces, particularly at the edges. This deformation induces stray light andleads to some optical loss. To generate the correct mirror angle, an auto-developer machineand a temperature-profile controllable hotplate chamber were used for stable baking and

development processes. However, more careful controls of room temperature and humidityare necessary to stabilize the other processes like spin-coating.The pitch of the fabricated optical redistribution was100 μm. Reducing the pitch to 50 μm is possible with current design and fabrication technology.

I. EVALUATION

The Si photonics die with optical redistribution was eval- uated as a device-under-test(DUT) sample. The insertion loss spectrum of the DUT was measured in a wavelengthrange of the S, C, and L bands (1460–1620 nm), as shown in Fig. 4. Broadband lightfrom a super luminescent diodewas polarized to TE polarization and provided as input to the Si waveguide end facet byusing a spherical lensed fiber. The light was propagated via the Si waveguide, mirror-basedcoupling, and polymer waveguide. The light output from the polymer waveguide wasreceived by a standard SMF witha cleaved end facet and measured by an optical spectrumanalyzer (OSA). A spherical lensed fiber was used for the small-MFD Si waveguide and acleaved facet SMF was used for the large-MFD polymer waveguide. To calculate theloss due to optical redistribution, the insertion loss of aSi photonics die without opticalredistribution was measured as a reference sample. During reference measurement, anotherspherical lensed fiber was used to receive light output fromthe sample. Consequently, lossdue to optical redistribution was derived by subtracting the insertion loss of the referencesample from that of the DUT. In this work, 1 8 splitter was integrated in the measuredtest pattern for measurement convenience. This splitter was not transparent in TM mode.Therefore, TM polarization was not evaluated. However, the optical redistribution composedof the mirror coupling and polymer waveguide can be low polarization dependent. The lowpolarization dependence of the bottom-side mirror was demonstrated in a previous work.The top-side mirror will also be low polarization dependent of a few percent differencesinceit is a simple metalized planar mirror. The polymer waveguide was also low polarizationdependent as reported in another previous workTo break down the 3.6-dB coupling loss, we prepared a simulation model of the fabricated

structure and simulated the optical coupling efficiencies while optimizing the modelparameters step by step. The simulation was performed using aphysical optics propagation

method presented in the commercial simulation software ZemaxOpticStudio. Firstly, to evaluate the stray light loss, total incoming power to the polymer waveguide end facet wascalculated. For the calculation, the power in a circle of 15-μm diameter, which was slightlylargerthan the size of the end facet, was integrated. The incoming power was 95%, so thestray light loss was 5%. Secondary, polymer-waveguide end-facet tilt angle was optimized inthe model and the efficiency was improved by 32%. Thirdly, the end-facet position wasoptimized. The end facet was in de-focus position. By moving the end facet close to focusposition, the efficiency was improved 19%. On the otherhand, misalignment losses for theother two directions were small enough to be ignored. Thus, the misalignment loss wasattributed from the de-focus condition. Finally, the MFD of the polymer waveguide wasoptimized and the efficiency was improved 37%. Remained 7% loss would be a part of theMFD mismatch loss and/or de-focus loss which cannot be optimized in the simulation. Thus,the tilt error, de-focus and MFD mismatch losses (32, 19 and 37%, respectively)were dominant factor. These losses can be decreased by optimizing the position, surfacecurvatures and tilt angle of the bottom side mirror. Using the initial prepared simulationmodel, the above three parameters were optimized. As the angle optimization, the x positionof the top-side mirror was also tuned. As a result, the coupling efficiency of -0.7 dB wasachieved in the simulation. Ultimately, the coupling efficiency, of -0.4 dB was also achievedby using a planar top-side mirrorwhich was not deformed.

I. CONCLUSION

The feasibility of optical redistribution, composed of two micro mirrors and a polymerwaveguide, was studied on a Si photonics die. The fabricated optical redistribution loss wascharacterized. The average loss of approximately 4 dB anda wavelength dependent lossof 1 dB were obtained for the wavelength range of 1460–1600 nm. The measured loss wasdecomposed into two loss factors, namely the polymer waveguide propagation loss and thecoupling loss of Si and polymer waveguides via the two micro mirrors. The coupling losswas approximately 3.6 dB on average, and the wavelength dependent loss was 0.65 dB overa 100-nm wavelength range. Thus, it was shown that the broadband optical redistributionwas available based on mirror-based optical coupling and polymer waveguide. An advancedtechnology to integrate the optical redistribution on a glass epoxy substrate, in which the Siphotonics die is embedded, will be developed in future works.

References:

[1] R. Dangelet al., “Polymer waveguides for electro-optical integration indata centers and high-performance computers,” Opt. Exp., vol. 23, no. 4,pp. 4736–4750, 2015, doi: 10.1364/OE.23.004736.

[2] (2018). Rockley Photonics Showcases Its in-Packaged Design atOFC. Gazettabyte. [Online]. Available: http://www.gazettabyte. com/home/2018/3/15/rockley-photonicsshowcases-its-in-packageddesign-at-ofc.html

Application Research of Virtual Reality Technology in Film and Television Technology

Student Name: Mr. SwapnilNikam

Class:SY Electrical Engineering

ABSTRACT

Nowadays, a new type of viewing mode - 360 degree panoramic film gradually appears in people's field of vision. The Spotlight Stories app developed by Google, the whole film of "HELP" is a 360° panoramic view. The gyroscope and accelerometer in the mobile phone are used to adjust the angle of the movie, and the sample can be rotated at the same time as the mobile phone is rotated. The angle you want to see. This is just the initial exploration of the panoramic film, which offers unlimited possibilities for the development of future panoramic films. In this paper, the author will study the new aesthetic experience characteristics brought by the application of virtual reality technology in the film. Therefore, the author has certain academic value for the research of image aesthetic experience under virtual reality technology. This paper has done a lot of preliminary literature research on the development of film technology, virtual reality technology and its characteristics, and the development history of film aesthetics. It has combed the development history of film technology, the change of film form, the development history of virtual reality image and its new specialty.

INDEX TERMS: Aesthetic Experience, Applied Research, Film and Television Technology, Virtual Reality Technology

I. INTRODUCTION

VR image (virtual reality image) is a virtual human-computer interaction method that uses virtual reality technology to generate a three-dimensional environment with computer system and sensor technology. It can make people immersive by simulating human sensory functions such as sight, hearing and touch. Among them, the viewer can look around in real life in a 360-degree virtual image environment. VR video works are still in the preliminary exploration stage, which changes the way traditional movies are produced, viewed and disseminated. Nowadays, when virtual reality technology enters the film, scholars' research on virtual reality movies mostly stays in the way of film creation and viewing. There is no research on the new aesthetic experience of virtual reality images. The viewing methods have brought revolutionary influences, giving us unexpected audio-visual feelings, especially the full application of technologies such as head-mounted devices and data gloves. Virtual reality technology has been fully developed, the material media of the narrative, and the audience. There are fundamental differences in the acceptance methods, the communication channels of images, and so on.

II. APPLICATION OF VR TECHNOLOGY IN FILM AND TELEVISION A. VIRTUAL REALITY TECHNOLOGY AND FILM ART

In the early stage of the development of virtual reality technology, it was widely used in the game field, relying on post-modeling software to construct a virtual game situation, and film and television art is an independent segment composed of a single lens, and then a complete story constructed by multiple independent segments . Although both games and movies have entertainment functions, compared with games, the art of movie and TV pays more attention to shooting. Highly immersive scene construction and shooting methods are the basis for realizing movie art. For film and television works produced by virtual reality technology, high-quality and superior-performance professional photography equipment such as 360-degree cameras, three-dimensional three-dimensional cameras, light field cameras, and motion capture systems that can be filmed in all directions must be used. Another main feature of virtual reality technology is “communication and interactivity”, which means that the audience can freely obtain desired objects, choose their own location, and observe in a certain virtual situation. The main purpose of virtual reality technology that can conceptually realize and strengthen language film and television works of art is to use and drive the audience’s vision and hearing to resonate, which is in line with the purpose of virtual reality technology to simulate real situations to allow the audience to generate rational or perceptual cognition. Coincidentally

B. THE IMPACT OF VR TECHNOLOGY ON THE FILM AND TELEVISION INDUSTRY (1) THE ROLE OF DIRECTOR IN FILM AND TELEVISION CHANGES UNDER VR TECHNOLOGY

This is because during the production process of VR, all the people who have nothing to do with the performance, such as the videographer, can’t be present. The director is the same, otherwise they will wear it. Therefore, the director can only express some opinions in the gap between the recordings as in the case of sports coaches, or re-shoot in the form of “cards”. To a certain extent, the director’s role is more like a drama director. He can design and dress in costumes, music, walking, props, lighting, performances, etc., but he can’t switch, fight, play, Over-the-shoulder lenses, focus, and montage techniques are used to express ideas, and all content depends on the actors’ performances.

(2) CHANGES IN STORY STRUCTURE, ROLES AND PERSPECTIVES IN FILM AND TELEVISION WORKS UNDER VR TECHNOLOGY

The perspectives, roles, and plot changes in movies based on VR technology reflect the impact of VR technology on the selection of stories and film scripts in the film industry.

There are great differences between traditional film and television works in terms of story structure, narrative angles, and story characters. VR technology film is a full-angle movie. The central axis is the eyes of the audience. The film and television story must be launched layer by layer with the eyes of the audience. It is also a unique advantage of VR technology film and audience interaction. This advantage is traditional film and television works. do not have. In the aspect of story structure and narrative perspective, VR technology film is more difficult. Because the audience has a large autonomy, it can watch from different angles. The film must consider all angles before it can give the audience A practical experience. This also represents the coherence of time and space in the structure of the story and the diversity of the narrative perspective is inevitable. The high-quality film and television scripts with many narrative clues combined with the superb creation and VR technology are also one of the problems that VR technology should focus on in the future. In addition, because of the broadness of choice, there are also differences in the time when the audience appreciates the same VR technology film and television works.

C. APPLICATION PROSPECT OF VR VIRTUAL TECHNOLOGY IN FILM AND TV ART

In recent years, although VR virtual technology has become a hot topic in the general public, this “popularity” is limited to the concept. VR virtual technology is not widely used in film and television art, and even domestic theaters have not been officially released. A movie made with pure VR virtual technology. Technology is a double-edged sword. VR virtual technology has certain advantages and has its own limitations. VR technology provides viewers with a full range of viewing experience, and because of the limitations of the device, the duration of the movie is too short, and the control is less than 20 minutes. After increasing the viewer’s free choice, the difficulty of VR film production will also change. Big, given this situation, the director tends to simplify the plot setting. Of course, VR virtual technology is not always a disadvantage. At this stage, the application of VR virtual technology in the field of film and television is mainly divided into three aspects: VR film and television experience, film and television short film and landscape film production. The director often uses the technical characteristics of VR itself, combined with the specific needs of film and television, to carry out some productions starting from VR movies, in order to meet the expectations of VR virtual technology in the new era. According to the survey, the audience's expectation of VR film and television is as shown in Table 1. It can be seen that most viewers are still looking forward to VR film and television.

TABLE 1

AUDIENCE STATISTICS ON VR FILM AND TELEVISION

Audience evaluation	ratio
Very rubbish	2.11%
general	8.23%
Very fresh form	37.61%
Very good	52.08%

III: VR FILM AND TELEVISION AESTHETICS NEW FEATURES

A. IMMERSION

No matter where you wear VR headlights, data clothing, data gloves and other immersive equipment, we can go skiing in the mountains, swimming in the sea, and go to the space to enjoy. In this "in the middle" immersion, the viewer has gained an unprecedented sense of freedom. This kind of freelance scholar Jiang Kongyang believes that it is the highest state of aesthetics. In addition to the beauty, the image can bring us pleasure, satisfaction and happiness. In addition to the sense of harmony, we should also bring us a sense of freedom. People often feel uncomfortable in daily life, but in VR images we can immerse ourselves in any world we want to immerse, and we can satisfy all of us in VR images. Imagine that this is not the vividness of abstraction, but a kind of experience, a kind of "real" experience

.

B. VIRTUALITY

Since the birth of 3D technology, all major commercial films have utilized this technology in their production. The status of 3D technology has become more and more solid, and people are constantly pursuing higher quality and more realistic film screening effects. At present, with the continuous maturity of computer technology, various special effects have brought a huge visual feast to the audience, and the senses of the audience have been greatly stimulated. The full use of virtual reality technology can further enhance the audience's experience, and the audience can get a more realistic experience in the virtual world, so that the experience can achieve better results

.

C. PERCEPTUAL

When virtual reality technology is used in film and television works, there is another important feature, perceptuality. When the audience experiences virtual reality technology, the information exchange between the technical device and the audience is dynamic, and the audience's perception is real-time. Therefore, the screen played by the related art device must be highly consistent with the viewer, so that the viewer can obtain a more realistic experience in the senses. Virtual reality technology can break the traditional film into the current state of the screen, so that the picture can be matched with the movement of the audience, and with the change of the audience’s movement mode, present a different and realistic picture.

IV. ANALYSIS OF THE NEW AESTHETIC CHARACTERISTICS OF VIRTUAL REALITY IMAGES

A. THE BEAUTY OF VR TECHNOLOGY IN FILM AND TELEVISION ART

(1) IMMERSION AND ENTRY

At the 2015 Game Developers Conference (Global Development Center, GDC for short), the “Walking in the Clouds” VR experience movie has greatly affected people’s worldview, as shown in Figure 1. (Photo from the Internet). When the viewers put on the helmet display device and entered the VR world of the movie, the thick rope under the foot has become the steel cable hanging between the 450 meters high-rise World Trade Center Twin Towers, and the head is the bustling New York street. In the ear is the whistling sound from the headphones. From the very beginning, the viewers began to tremble involuntarily because of fear. Although, they know that in the real space, the ropes are not suspended in the sky, even if the feet are empty, it is absolutely safe. However, through this realistic immersion, the viewer still unconsciously responds according to the high-altitude environment seen in the film. Therefore, the new experience brought by the film and television art works using VR technology brings a strong sense of reality to the viewers.

FIGURE 1 Screenshot of the movie “Walking in the Cloud”

(2) INTERACTIVITY AND BODY SHAPING

As shown in Figure 2 (picture from the network), the “Top Player” movie shown in the 3D effect movie, everyone is immersed in the virtual world with VR devices at home, people can shape in this virtual world In any role role, all the senses of touch, power and so on can be felt through advaced technology equipment. In the whole process of interaction, the viewers not onnly communicate with the film and television art works using VR technology, but also bring people’s entire physical and mental potential to the full play, so that the viewers can participate in the film and television works to the maximum extent. In the aesthetic activities.

FIGURE 2 Movie “number one player” screenshot

B. THE FORM OF VR TECHNOLOGY IN FILM AND TELEVISION ART

(1) 3D EFFECT MOVIE

After the release of Cameron’s 3D effect film “Avatar” in 2009, it ignited the enthusiasm of the global viewers for 3D effect films, which is undoubtedly an epoch-making work. As shown in Figure 3 (picture from the Internet), the film “Avatar” is presented to the viewers in a fairytale fantasy world, which is infinitely imaginative.

A Pandora planet that is different from the real world in which people live, the species is also in a variety of ways, and is perfectly integrated with the environmental space. A large number of magnificent 3D effect images appear in front of the viewers, and the overlapping of depth of field makes the layering clear. Cameron’s rich

FIGURE 3Movie “Avatar” screenshot

imagination and visual impact are enhanced by the use of advanced technology to cater to the viewer’s inner world. The 3D effect film uses VR-related playback equipment and perspective principle to create a large depth of field effect with obvious stereo effect. It is equipped with 5.1 stereo surround sound, which further enhances the sense of spatial depth from the auditory level, allowing the viewer to be at a certain level. It creates an immersive feeling.

(2) CGVR VIDEO

CGVR is the abbreviation of Computer Graphics. It is all 2D or 3D graphics technology drawn by Flash, Photoshop, Maya, 3DsMax and other software. Compared with the real shooting method, the film produced by the CG production method can seamlessly splicing each scene without considering the misalignment of the stitching of the photographed material. A CGVR animated film called “Pearl”, as shown in Figure 4 (picture from the Internet), was nominated for the 85th Oscar for best animated short film. The film is about 6 minutes long and tells the story of a musician driving his country across the country with his daughter. The whole film does not have a panoramic view of the jewels, and there is no huge scene of shocking. Instead, the perspective of the viewer is fixed at the position of the co-pilot of the car, and the flow of scenery outside the window is reflected by the simulation of the squatting, but the view is reflected. The shadow can also extend the head out of the window to enjoy the scenery. To a certain extent, it can reduce the limitations imposed by real shots and enrich the viewers’ audiovisual needs.

FIGURE 4 Cartoon “Pearl” screenshot

V. CONCLUSIONS

(1) In this paper, the author will study the new aesthetic experience characteristics brought by the application of virtual reality technology in the film. Therefore, the author has certain academic value for the research of image aesthetic experience under virtual reality technology. This paper has done a lot of preliminary literature research on the development of film technology, virtual reality technology and its

characteristics, and the development history of film aesthetics. It has combed the development history of film technology, the change of film form, the development history of virtual reality image and its new specialty. The new aesthetic characteristics of virtual reality images are summarized by case study method and comparative research method.

CMOS-Compatible Silicon Photonic Sensor for Refractive Index Sensing Using LocalBack-Side Release.

Student Name: Mr Anil Ganeshwade

Class:SY Electrical Engineering

Abstract:

Silicon photonic sensors are promising candidates for lab-on-a-chip solutions withversatile applications and scalable production prospects using complementary metal-oxidesemiconductor (CMOS) fabrication methods. However, the widespread use has been hinderedbecause the sensing area adjoins optical and electrical components making packaging and sensor handling challenging. In this work, a local back-side release of the photonic sensor isemployed, enabling a separation of the sensing area from the rest of the chip. This approachallows preserving the compatibility of photonic integrated circuits in the front-end of line andmetal interconnects in the back-end of line. The sensor is based on a micro-ring resonator andis fabricated on waferlevel using a CMOS technology. We revealed a ring resonatorsensitivity for homogeneous sensing of 106 nm/RIU.

Index Terms: Silicon photonic sensor, silicon photonics, integrated photonics, refractiveindex sensing, photonic biosensor.

INTRODUCTION

SILICON-based photonic biosensors integrated into a semiconductor chip technology can lead to significant advances in point-of-care applications, food diagnostics, and environmental monitoring through the rapid and precise analysis of various substances. In recent years, there has been an increasing interest in sensors based on photonic integrated circuits (PIC) because they give rise to cost-effective, scalable and reliable on-chip biosensors for a broad market. The PIC technology employs typically silicon-on-insulator (SOI) wafer, which is the most attractive approach from a commercial point of view since it provides a scalable platform for mass production using complementary metal-oxide semiconductor (CMOS) fabrication processes. Once the photonic chip is fabricated, it can be used for homogeneous sensing of refractive index variations or it is employed for surface sensing by coating the silicon waveguide with a covalently attached sensing layer. The sensing layer determines the specific detection and, hence, the application. This step, however, is independent of the fabrication of the chip, making the PIC technology based on SOI wafer attractive for both, science and industry. A further advantage of PIC-based biosensors is the possibility to realize sensor arrays using, e.g., an inkjet surface functionalization process [3]. This allows for the detection of several substances in parallel (multiplexing) [4]. During the last two decades, integrated photonic sensors have been intensively studied in terms of sensitivity and reliability [5]. However, the bottle-neck for a transfer from laboratory to industry is the position of the sensing area, since it adjoins optical and electronic components. This prohibits cost-effective packaging and makes the sensor handling impractical.

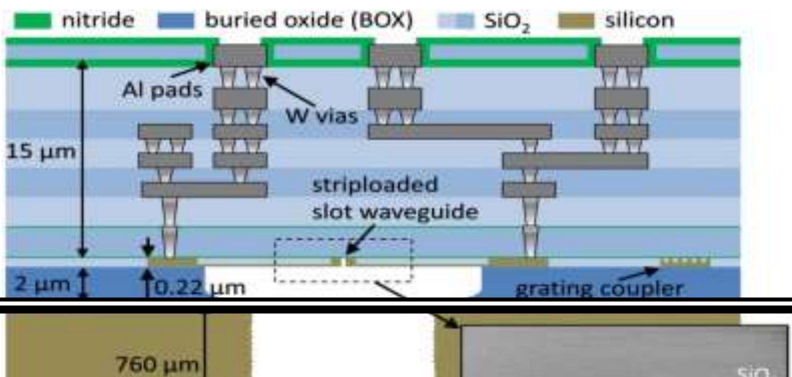

SENSOR I

Figure 1: Schematic cross-section of a back-side released silicon slot waveguide with complete back end of line.

The pho .ng 200 mm SOI wafer with a 220 nm thick c-Si on top of a 2 µm buried oxide, as shown in Figure 1. The idea is to shift the sensor from the crowded and water-sensitive front-side of the chip to the back-side. This is realized by a local back-side release, following the work in. In this case, the photonic sensor is released from the wafer back-side by a dry etch followed by a wet etch to locally remove the silicon substrate and the buried oxide, respectively. To protect the back-end of line against the relatively long etching time and to enable a back-side integration on wafer-level, the passivation of the top metal pads is modified following the procedure reported in. It is worth to mention that the lowest grating coupler loss of 4 dB was achieved with the fabrication flow using a standard passivation module, while a 5 dB grating coupler loss was observed with the adjusted passivation module. For the local back-side etch (LBE), a planarization of the back-side and the deposition of Si O2 as hard mask is required. The hard mask is patterned with DUV lithography and reactive ion etching, while deep reactive ion etching process is employed to etch the 760 µm silicon substrate. To test the viability of the fabricated photonic sensor, we perform homogeneous sensing experiment to evaluate the sensitivity. The ring resonator sensitivity for homogeneous sensing is defined as $SR\ R = \lambda res\ n\ f$, (1) where λres refers to the resonance wavelength shift and $n\ f$ to the refractive index change of the fluid. Developing application-specific sensors is typically a balancing act between sensitivity and optical losses traded off against each other within the limitations of the present fabrication flow. On the one hand, narrowing the line width (FWHM) reduces the detection limit. This can be achieved by lowering optical

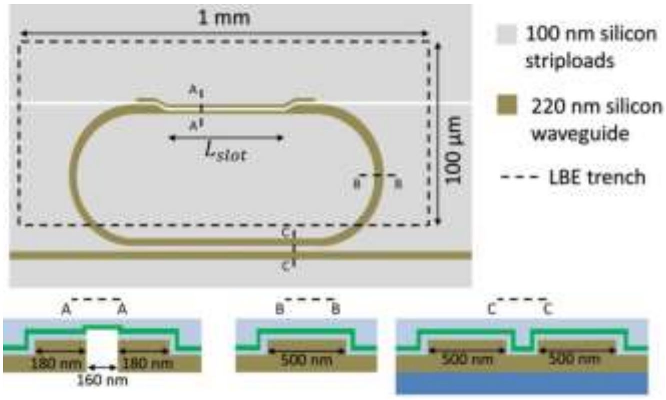

Figure 2 : Schematic top view of the ring resonator with cross-sections of different waveguides.

losses within the ring resonator. On the other hand, lower losses are primary observed through strongconfinement inside the silicon waveguide, which leads to a lower interaction with the fluid. As a consequence, the ring resonator sensitivity is reduced at the same time. One strategy to find a tradeoff is the use of a partially slotted ring resonator.

Figure 3 plots the relative effective refractive index over the refractive index of fluid. The relative effective refractive index is defined as neff = neff (C) – neff (0wt%), where C represents the concentration of NaCl in DI water. The waveguide sensitivity can be deduced from the slope of the linear fitting function. It is revealed that the slot waveguide with thinner strip loads (50 nm) exhibits the highest waveguide sensitivity of SW G = 0.323, while the rib waveguide shows no significant dependence of the waveguide sensitivity on the strip load height. However, due to fabrication limitations, we used strip loads with a thickness of 100 nm. Figure 3 shows the optical field distribution of a back-side released slot and rib waveguide having the employed waveguide geometries.

RESULTS

Figure 4 shows the observed optical spectrum of the backside released micro-ring resonator, measured with a tunable laser having a wavelength resolution of 5 pm. We inferred an extinction ratio of E R = 20 dB and a full width at half

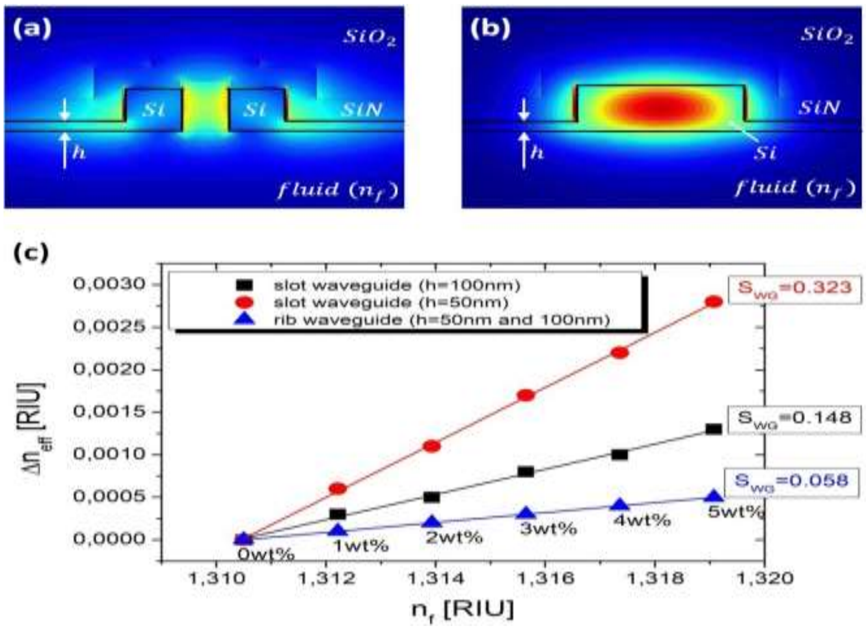

Figure 3 :Optical field distributions in a slot

(a) and rib waveguide

(b)atwavelengthof1550nm.

Relative effective refractiveindexasafunctionoftherefractive index of the fluid is shown in (c). NaCl in DI water was consideredasfluid havingdifferentconcentrations,asindicated in the graph.

Fig. 4. Optical spectrum of the back-side released micro-ring

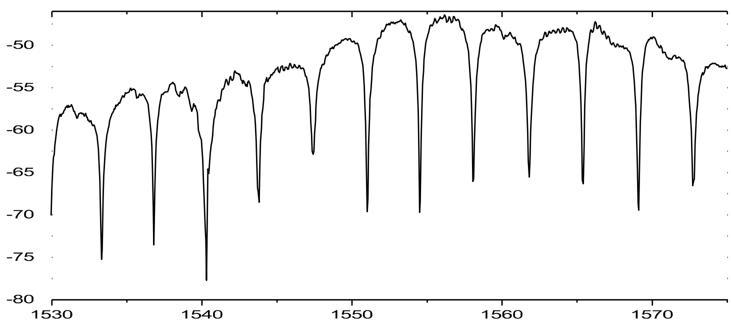

resonator.maximum of FWHM = 0.55 nm ($Q = \lambda/FWHM \approx 2800$) from this figure. The sample is fixed on a hot plate in this experiment, and by tuning the temperature, we have revealed a temperature sensitivity of ST = 92 pm/K, which is comparable with a similar ring resonator that has been opened from the top [14]. The experimental results of this experiment are shown in Figure 5. As proof of principle, we have performed homogeneous sensing experiments with different concentrations of NaCl in DI water. For this experiment, we employed a super luminescence diode and an optical spectrum analyzer with a wavelength resolution of 30 pm, while the photonic chip is fixed on a 3D-printed sample holder with a fluid reservoir. The grating coupler is TE-polarization selective and were used in order to couple the light from a single-mode fiber into the chip. TE-mode operation is achieved by maximizing the output signal through a paddle-style fiber polarization

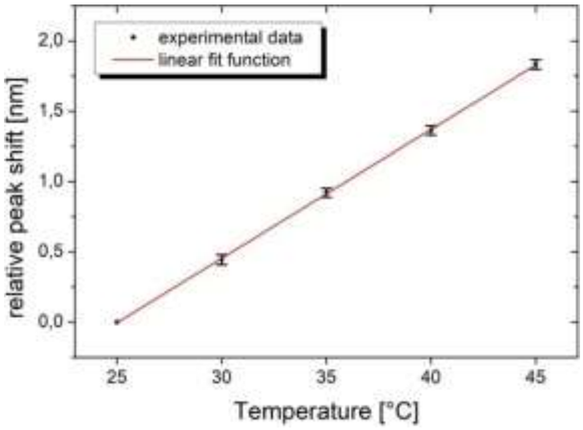

Fig. 5.Relative peak shift as function of the temperature.

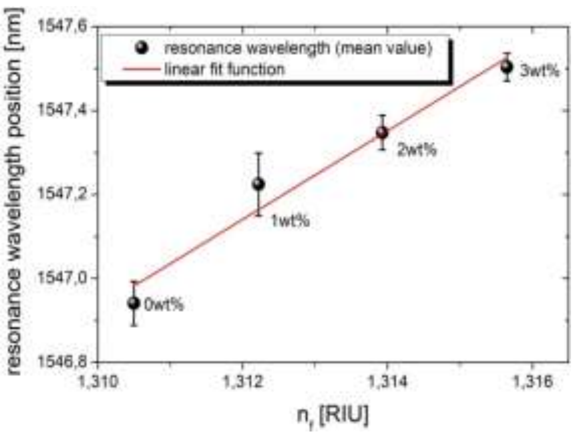

Fig. 6. Resonance wavelength shift as function of the refractive index of the fluid

controller. Liquids with a different weight percentage of NaCl ranging from 0wt% to 3wt% were dropped onto the silicon photonic sensor using a pipette. The refractive index n f of the NaCl solved in DI water at different concentrations C(wt%) and at a wavelength of 1550 nm can be calculated by n f (wt%) = 1.3105 + 0.17151 × C(wt%)/100. For the selected concentrations from 0wt% to 3wt% the refractive index of the solution hence ranges from 1.3105 to 1.3157. We used the same ring resonator for all measurements. After each measurement, the chip was carefully cleaned and dried. To characterize the homogeneous sensing, we plotted the resonance wavelength as a function of the refractive index of the fluid (NaCl in DI water) in Figure 6. Through a linear regression, we have deduced a ring resonator sensitivity of SR R = 106 nm/RIU, which is comparable with values reported for similar micro-ring resonators released from the front-side.

CONCLUSION

For the first time, we have presented an approach to fully integrate silicon photonic sensors in a PIC technology, having a complete back-end of line. A local back-side etch process is employed to release the photonic sensor from the backside of a 200 mm SOI wafer. As proof of principle, refractive index sensing (homogeneous sensing) was demonstrated using a partially slotted ring resonator. A ring resonator sensitivity of SR R = 106 nm/RIU is revealed, which is similar to values observed with front-side released sensors having a comparable resonator geometry. The CMOS-compatibility and the possibility to use the complete back-end of line to connect photonic sensor elements with electronic devices on the same chip as well as the separation of the photonic sensor from optical and electrical connections make the back-side integration concept attractive for future sensor systems.

References:

[1] E. Luan, H. Shoman, D. Ratner, K. Cheung, and L. Chrostowski, “Silicon photonic biosensors using label-free detection,” Sensors, vol. 18,no. 10, p. 3519, Oct. 2018. [Online]. Available: https://www.mdpi.com/1424-8220/18/10/3519

[2] A. Rahim et al., “Open-access silicon photonics platforms in Europe,”IEEE J. Sel. Topics Quantum Electron., vol. 25, no. 5, pp. 1–18,Sep. 2019.

Bio-Nano-Composite Materials Constructed With Single Cells and Carbon Nanotubes: Mechanical, Electrical, and Optical Properties

Student Name: Mr.MoinMujawar

Class: B.Tech Electrical Engineering

Abstract:

Here, we report a procedure to obtain novel artificial materials using either fungal or isolated tobacco cells in association with different percentages of carbon nanotubes. The electrical, mechanical, and optical properties of these materials have been determined. The produced bio-nano-composite materials have linear electrical characteristics, high temperature stability up to 180 ◦C, linear increase of the electrical conductivity with increasing temperature and, in one case, also optical transparency. Using tobacco cells, we obtained a material with low mass density and mechanical properties suitable for structural applications along with high electrical conductivity. We also present theoretical models both for their mechanical and electrical behavior. These findings report a procedure for the next generation bio-nano-composite materials.

Index Terms—Bio-materials, bio-nano-technology, electrical materials, structural materials.

I. INTRODUCTION :

Biological components from different sources (e.g., collagen) have been used to obtain nanostructured materials that are employed as synthetic scaffolds into which biological tissues have been applied. Bio composite materials for mechanical or electrical applications have also been produced. However, a procedure to generate bio-nano-composite materials composed of cells and carbon nanotubes for engineering applications has not been reported yet. The development of synthetic biomaterials will effect greatly the production of new electronics and artificial materials. Scaffolds that support cell growth and simultaneously monitor cell activities have been described. Biodegradable three-dimensional (3-D) structures that serve as short-term supports for cells and new tissue growth have been also formed with hydrogel using inert synthetic molecules such as poly(ethylene glycol). Synthetic gels mediate the delivery of trophic factors for neural cell repair. An artificial hetero-cellular 3-D architecture has been used also to monitor the molecular behavior of cancer cells.

II. MATERIALS AND METHODS

The different types of materials produced are as follows:
1) BY-2 tobacco cells with 20% of a 1% sodium dodecyl sulfate (SDS) solution saturated with multi-walled carbon nanotubes (MWCNTs), (tobacco/20-MWCNTs); 2) C. albicans with 6.6% of 1% SDS solution saturated with MWCNTs (Ca/6.6-MWCNTs); 3) C. albicans with 20% of a 1% SDS solution saturated with MWCNTs (Ca/20-MWCNTs). To obtain a Ca/20-MWCNTs material, Candida yeast phase cells grown at 25 ◦C in RPMI medium (Sigma-Aldrich, St. Louis, MO, USA) were collected at an absorbance of 0.36 OD600 and used for the experiments. To obtain the Ca/6.6-MWCNTs material, yeasts were grown at 25 ◦C in YPD (yeast peptone dextrose) medium. Between 3 and 6 independent cells/MWCNTs suspensions were produced and each analyzed individually. Commercially available CNTs (nonmodified type “3100” multiwalled CNTs, Nanocyl) were used in a solution with SDS as described earlier.

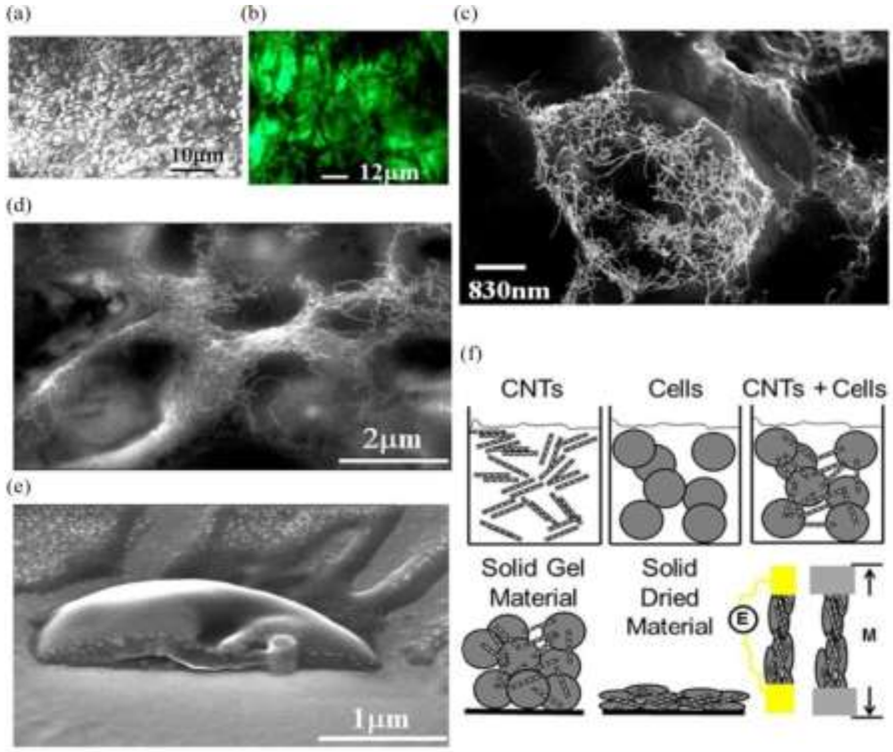

Fig. 1.Structure and preparation of cell/MWCNTs tissues.
(a) Microscopy image of dehydrated Ca/20-MWCNTs artificial tissue (SEM image, magnification 2 000×).
(b) Optical microscopy image of dehydrated tobacco/20-MWCNTs artificial tissue (magnification 800×).
(c) Detail of Ca/20-MWCNTs interaction (SEM image) (magnification 12 000×). (d) SEM image of Ca/20-MWCNTs (magnification 15 000×) with MWCNTs acting as artificial adhesins.
(e) SEM image of FIB cut section of a dehydrated isolated cell of C. albicans (Magnification 35 000×).
(f) Drawing of the process used to obtain the materials and the sample geometries for electrical and mechanical characterization.

III. RESULTS AND DISCUSSION

Here, we report, as a proof of concept, that single cells of C. albicans and isolated tobacco cells (BY-2), either one in association with MWCNTs, form artificial "tissue" materials. MWCNTs allow the formation in vivo of a structured gel-like “tissue” by creating a tight network of tubes that act as artificial “adhesins”. Both Candida and isolated tobacco cells do not have the intrinsic capacity to grow as tissue. As seen in microscopic images [see Fig. 1(a)-(d)] cells of the composed materials are interconnected by CNTs. After the in vivo formation, the materials were dried and the dehydrated cells still acted as a stable matrix for the MWCNT network. Only a fine powder of dead cells that pulverized was obtained when cells in the absence of CNTs were dried in a control experiment.

Fig. 1(f) shows a sketch of the used procedure. When observed by optical and by SEM the material resembled an artificial tissue composed of highly packed cells [see Fig. 1(a),(b)]. We previously reported that MWCNTs are inserted into the cell wall of C. albicans. Figs. 1(c) and (d) shows that MWCNTs surround the cells acting as artificial adhesins.

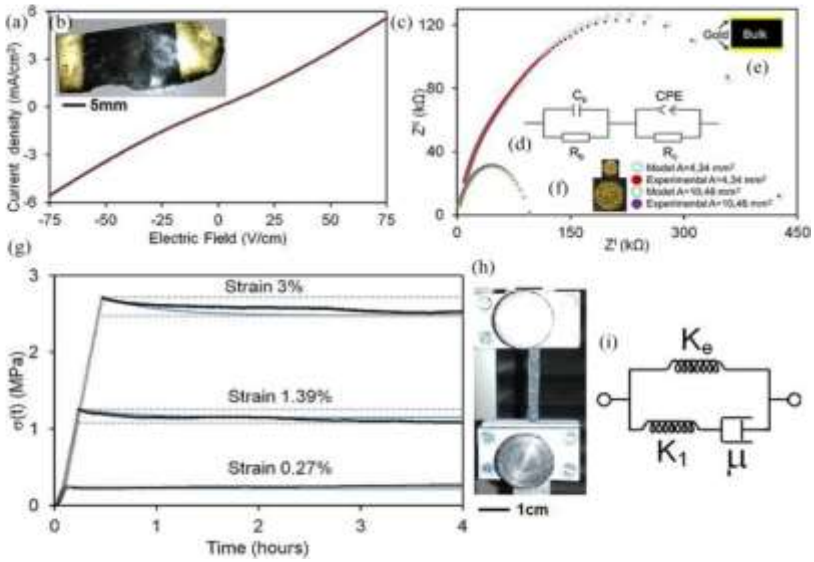

Fig. 2. Electrical and mechanical characteristics of tobacco/20-MWCNTs samples.

(a) Electric field versus current density characteristic of the
material.

(b) Photograph of the sample with coplanar sputtered gold electrodes.

(c) Real part versus imaginary part of the electrical impedance:
reddotsindicate impedance spectroscopy relative to larger contacts,blue circlesindicate model simulation, violet dots indicateimpedance spectroscopy relative to smaller contacts, green circlesindicate model simulation.
(d) Schematics of the electrical model of the material.
(e) Cross section drawing of the sample sandwiched between gold
contacts.
(f) Picture of the top gold contacts
(g) Black lines show the relaxation test for three levels of steadystrain 0.27%, 1.39%, and 3%. Blue lines: fit with SL model; dashedlines are the initial and the long term levels of stress.
(h) Photograph of a tobacco/20-MWCNTs bar during mechanical tests.
(i) SL model schematics with K1 = E−Ke, Ke = 82.51 MPa,
μ = 16.08 GPa× s.

Fig. 1(e) shows the effect of cell dehydration as revealed by their “ghost cell” appearance. Using FIB/SEM, we cut a section of a dried isolated cell without CNTs and obtained an image of the treated cell with the incorporated SEM. Thus, we can conclude from these microscopic analyses that CNTs allow the formation of an artificial tissue-like material composed of dehydrated cells interconnected with MWCNTs.

Fig. 2 shows the electrical characteristics of tobacco/20- MWCNTs material. For this purpose, we sputtered coplanar gold electrodes on the ends of a material bar [see Fig. 2(b)] and determined the electric field versus current density characteristics of the material [see Fig. 2(a)].

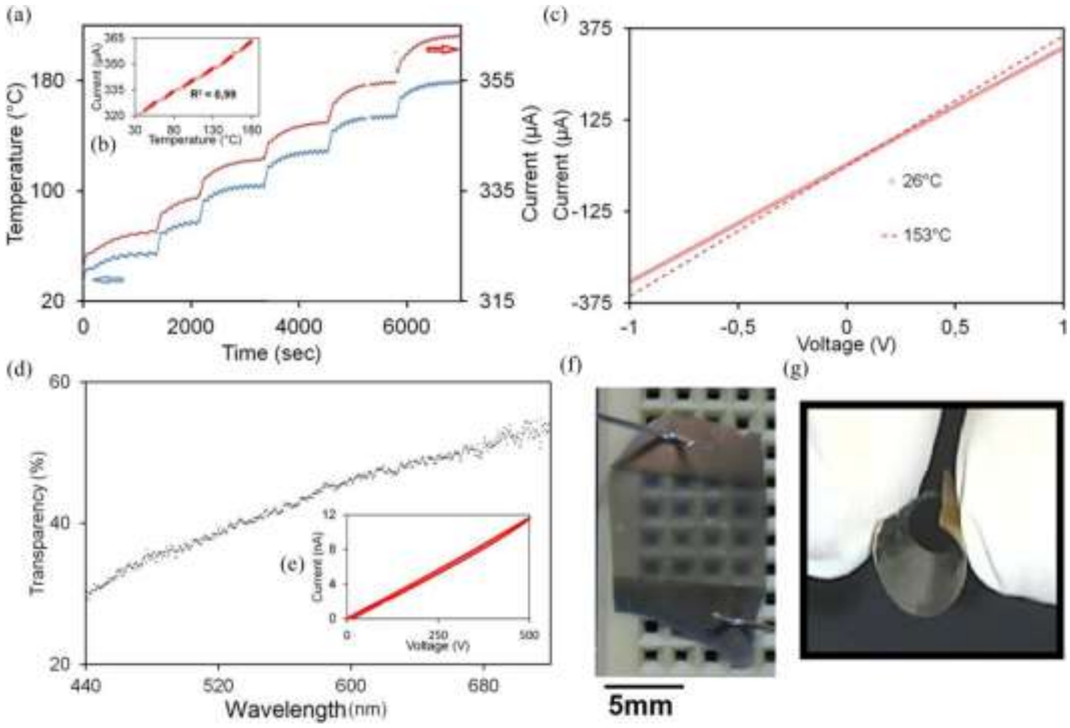

Fig. 3. Tissues thermo-electrical characteristics and optical transparency of Ca/MWCNTs.

(a) Ca/20-MWCNTs: temperature (indicated by the blue line) and corresponding sample current (indicated by the red line) versus time measured during a step-stress test up to 180 ∘C.

(b) Ca/20-MWCNTs: current–temperature characteristics of the sample.

(c) Ca/20-MWCNTs: current–voltage characteristics at 26∘ (red circles) and 153 ∘C (dashed line).

(d) Ca/6.6-MWCNTs: optical transparency spectrum in the visible range.

(e) Ca/6.6-MWCNTs: current–voltage characteristics up to 500 V. (f) Photograph of the Ca/6.6-MWCNTs on an electrical components breadboard.

(g) Photograph of Ca/6.6-MWCNTs of a thin film bent between two fingers.

IV. CONCLUSION

In summary, we have established a procedure to obtain bio nano-composite materials constructed with cells and carbon nanotubes. These bio-materials are appropriate for electric engineering applications since they have performances comparable to existing CNT-composite materials. Further, our bio-nano-composite materials have values of strength and stiffness that make such a material also suitable for structural applications.

References:

[1] B. Tian, J. Liu, T. Dvir, L. Jin, J. H. Tsui, Q. Qing, Z. Suo, R. Langer,D. S. Kohane, and C. M. Lieber, "Macroporous nanowire nano-electronicscaffolds for synthetic tissues," Nat. Mater., vol. 11, pp. 986–994, Aug.2012.

[2] G. D. Nicodemus and S. J. Bryant, "Cell encapsulation in biodegradablehydrogels for tissue engineering applications," Tissue Eng. B, Rev., vol. 14,pp. 149–165, Jun. 2008.

[3] J. S. Katz and J. A. Burdick, "Hydrogel mediated delivery of trophic factors for neural repair," Wiley Interdiscip.Rev.vol. 1, pp. 128–139, Feb. 2009.

MyoBio: An Automated Bioreactor System Technology for Standardized Perfusion-Decellularization of Whole Skeletal Muscle

Student Name: Ms.RutujaEkate

Class: B.Tech Electrical

Abstract—Objective: Decellularizing solid organs is a promising top-down process to produce acellularbioscaffolds for 'de novo' regrowth or application as tissue 'patches' that compensate, e.g., large volumetric muscle loss in reconstructive surgery. Therefore, generating standardized acellular muscle scaffolds marks a pressing area of need. Although animal muscle decellularization protocols were established, those are mostly manually performed and lack defined bioreactor environments and metrologies to assess decellularization quality in real-time. To close this gap, we engineered an automated bioreactor system to provide chemical decellularization solutions to immersed whole rat gastrocnemius medialis muscle through perfusion of the main feeding arteries. Results: Perfusion control is adjustable according to decellularization quality feedback. This was assessed both from (i) ex situ assessment of sarcomeres/nuclei through multiphoton fluorescence and label-free Second Harmonic Generation microscopy and DNA quantification, along with (ii) in situ within the bioreactor environment assessment of the sample's passive mechanical elasticity. Conclusion: We find DNA and sarcomere-free constructs after 72 h of 0.1% SDS perfusion-decellularization. Furthermore, passive elasticity can be implemented as additional online decellularization quality measure, noting a threefold elasticity decrease in acellular constructs. Significance: Our MyoBio represents a novel and useful automated bioreactor environment for standardized and controlled generation of acellular whole muscle scaffolds as a valuable source for regenerative medicine.

Index Terms—Biomechatronics, bioreactors, tissue engineering, decellularization, skeletal muscle.

I. INTRODUCTION

PATIENTS suffering from irreversible muscle loss, either due to trauma, necrosis or tumor ablation, currently exclusively rely on the use of autologous muscle grafts (involving, e.g., M. gracilis, M. latissimusdorsi) [1], which often leads to impaired functional recovery and reduced motility/strength even after prolonged physical rehabilitation [2], [3]. Unfortunately, more than 10% of all reconstructive surgeries eventually fail due to graft infection [4], and are also accompanied by the risk of donor site morbidity [2]. To overcome such limitations of autologous transpositions [1], [2], [5], new methods in tissue engineering aim to find sustainable alternatives for heterologous transplantation approaches [6]–[8]. In that regard, a promising approach is the bio-engineering of organs via tissue-printing (bottom-up), [9]–[11] or the recreation of acellular scaffolds that serve as either meshwork to re-engineer organs from patient recipient cells (top-down) [12], or for direct implantation as biomimetic 'muscle tissue patch' to enhance muscle regeneration [13], [14]. Particularly, the top-down approach to obtain bio-scaffolds from previously intact organs reflects a promising method as it conserves the vascular network and the specific tissue-inherent architecture which is usually challenging to achieve in bio-printing and has not yet been convincingly demonstrated in bottom-up processes [15]–[17].

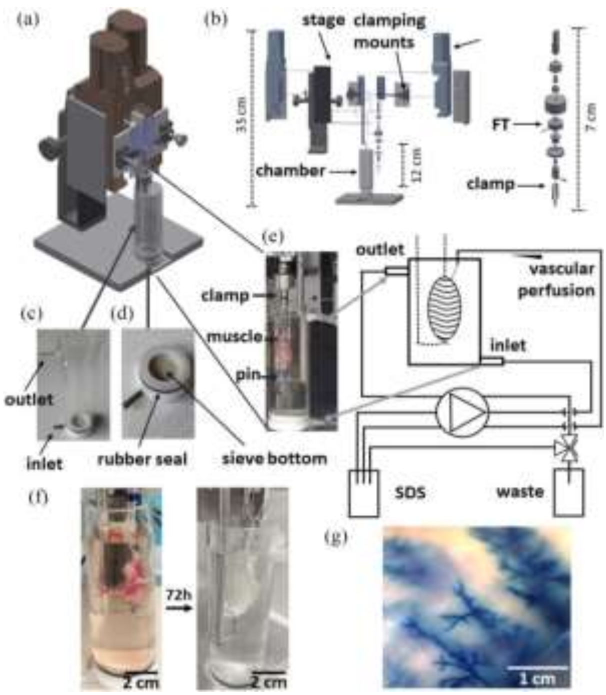

Fig. 1.v MyoBio system setup and flow chart for automated muscle decellularization.

(a) CAD construction drawing of the MyoBio bioreactor with its key components highlighted and named in the (b) explosion drawing to the right. (c) and (d) display an enhanced view of the reactor chamber and the sealing sieve bottom. (e) shows a photograph of a clamped muscle sample in the reactor chamber during system operation. A flow chart of the system is given to the right. The reactor is either operated in continuous flow mode for perfusion-decellularization (valve directs to SDS) or in batch mode (valve directs to waste) for future cell re-seeding experiments. A hose pump flushes the system with 0.1% SDS (w/v) in ddH 2 O through both, the chamber inlet and the muscle's vasculature. In perfusion or loop configuration, the SDS reservoir also serves as a waste flow. (f) After 72 h, the muscle has predominantly lost its myoglobin and presents translucent. (g) Flushing the vasculature with methylene blue confirmed the integrity of the vascular system within the isolated muscle.

II. MATERIAL AND METHODS

A. MyoBio Bioreactor System

1) Hardware Components: The MyoBio bioreactor system (Fig. 1(A)) is designed to meet the demands of a fully automated platform to create acellular skeletal muscle ECM scaffolds which may be further used as muscle patches in transplantation medicine or as a precursor for recellularization bioprocess optimization. The system is composed of two linear motors (L-406, PhysikInstrumente (PI) GmbH & Co. KG, Karlsruhe, Germany) that allow to adjust the prestretch to the length of each individual muscle and to perform mechanical stimulation and biomechanical characterization of the sample during decellularization. Each motor spans an actuation range of 25 mm, allowing a maximum of 50 mm stretch/actuation. Both motors are connected to a manual Z-stage for initial height adjustment. Spring fastening clamping mounts were installed to facilitate pin attach- and detachment to simplify sample mounting and transportation. One of these pins is composed of a force transducer (8411, burster, Gmbh& Co. KG, Gernsbach, Germany, Fmax = 10 N) in series with a bulldog clamp to which the proximal tendon of the sample muscle (M. gastrocnemius medialis) is attached. The other pin features a rod with a notch to fix the distal tendon (Fig. 1(B)). A central feature of the MyoBio is a glass cylinder that forms the reactor chamber (Fig. 1(C)). It is composed of a detachable sieve bottom which is sealed with a Teflon ring (Fig. 1(D)).
2) Software and Systems Electronics: Both linear actuators are connected in a daisy chain configuration to the C863 Mercury Servo Controller (PhysikInstrumente (PI)) and transmit serial data via USB to the CPU. The entire control software was written in C and Python which also

governs reading out FT data. A custom-made GUI allows controlling the motors manually before mounting and to set up different biomechanical stretch stimuli to execute during the decellularization protocol. Various biomechanical stimulation or testing methods can be chosen from, with a wide range of additional adjustments, like wave-form stimuli (e.g. saw-tooth wave, sine wave, etc.), conditionals (stop at a certain tissue compliance, at a maximum/minimum passive restoration force or at a defined time-point), biomechanical testing methods (RLT-curves, etc.), methods with force-feedback dependence or other methods important for user-handling (bug-fix mode, pause, end methods, etc.). Furthermore, the flow-rate and fluid direction of the hose pump is also controlled via the GUI.

A. Animal Model and Muscle Preparation

Donor animals were male Lewis rats (rattusnorvegicus) of ca. 300 g weight. Anesthesia was induced by inhalation of 4% isoflurane under spontaneous breathing with butarphenol and meloxicam as an analgetic. All animal procedures were performed in accordance to the German regulations for the care of laboratory animals at all times. Experiments were approved by the local animal care committee and government. Rats were in supine position and gastrocnemius muscle was prepared through an incision on the anterior hind limb. Adductor muscles were dissected to expose gastrocnemius muscle with its insertions at the femur (proximal) and the achilles tendon (distal). All feeding vessels except for the popliteal artery and vein as the main pedicle of the gastrocnemius muscle were ligated. The medial head of the gastrocnemius was dissected from the lateral head and the proximal and distal insertions were detached from the femur and the achilles tendon, respectively.

B. **Biomechanical Assessment During Perfusion-Decellularization**

During perfusion-decellularization with 0.1% SDS (w/v) for approx. 72 h, RLT-recordings were carried out to monitor the change in passive elasticity while the muscle was continuously freed of its cellular components. To contrast these changes, we conducted RLT assessments to stretch the preparation up to 115% of its resting length at a velocity of 2 $\mu m\ s^{-1}$ which is close to the quasi-static stretch regime.

C. **Optical Clearing**

The muscle (either native or decellularized) was pinned onto a silicone-elastomer-coated Petri dish (Sylgard, Dow Corning, Midland, Michigan, USA) and immersed in 4% paraformaldehyde (PFA). The composite was then placed on a shaker for 2 h at 30 rpm at room temperature (RT). To subsequently clear the muscle sample, it was immersed in 10 ml of increasing 2,2- Thiodiethanol (TDE) concentrations (volume fractions used: 30%, 50%. 70%, and 80%) [45]. Each step was performed for 4 h on a shaker at 30 rpm at RT. Samples were stored in 80% TDE at 4 ∘C overnight.

D. **Two-Photon Second Harmonic Generation Microscopy:**Amultiphoton system (TriM-scope II; LaVisionBioTec GmbH; Bielefeld) with a femtosecond pulsed Ti:Sa laser was used to image muscle samples (water immersion objective (25x Zeiss, Jena, Germany)) for myosin-II and collagen-I structures. The Ti:Sa laser was tuned to a wavelength of 810 nm to simultaneously excite both proteins. A photomultiplier was used with a band-pass filter at 405 nm ±10 nm. Images wereacquired with a total resolution of 1,024 x 1,024 or 512 x 512 pixels, respectively. Images were processed in Image J (National

Institute of Health, Bethesda, Maryland, USA) to apply gamma correction, adjusted brightness for enhanced visualization, and further colorization with a red & blue lookuptable.

B. Scanning Electron Microscopy

Microscopy slides were silanized in a custom-manufactured 3D slide holder made of polytetrafluorethylene. Before treatment, all microscopy slides were cleaned for 10 min in pure isopropanol (100%) to minimize artifacts during SEM imaging. Subsequently, the slides were incubated in 2% (3- Aminopropyl)triethoxysilane (APTES) for 10 min and further treated with pure acetone (100%) twice. Furthermore, the slides were washed thrice with millipore water for 10 min each and dried for a minimum of 24 h before further use. SEM imaging was performed with the JSM-IT300LV electron microscope (Jeol Ltd, Tokyo, Japan) at a low vacuum. Muscle cryosections were collected on silanized 20 mm x 20 mm microscopy slides, coated with indium tin oxide (ITO) and washed with a solution of 1% osmium in 0.1 M cacodylate buffer (1:1) for 2 h. Dehydrating the samples was perfomed with an ascending alcohol series, followed by further treatment with acetone, before drying them in a critical point dryer (Leica EM CPD 300, Wetzlar Germany). Finally, the samples were spotted with gold particles in a low vacuum coater (Leica EM ACE 200, Wetzlar Germany). Images received no further adjustments.

III. RESULTS

The engineering of an automated bioreactor system to create cell-free muscle scaffolds required a highly established decellularization technique, which allows system validation with an easily executable protocol. As such, the chosen decellularization method (0.1% SDS in ultra-pure water for 72 h) satisfied the ease-of-use criterion and yielded a better scaffold quality as compared to other decellularization techniques in skeletal muscle tissue (data not shown). For an adequate validation, our MyoBio was applied to decellularize gastrocnemius medialis muscle over 72 h of automated system operation.

A. Critical Bioreactor Improvements Stabilized the Decellularization Process

Initial experiments revealed the importance of a centralized and stable positioning of the perfusion tube to allow a strainrelieved perfusion. With the loss of structural proteins inside of the vascular system, already small vertical or horizontal forces were enough to lose the vascular tubing and lead to the inevitable abortion of the experiment. This was especially critical during biomechanical experiments.

B. B. 0.1% SDS Automated Perfusion-Decellularization Achieved a Profound Loss of Cellular Components

Fig. 2 displays Second Harmonic Generation images to compare native muscle to osmotic shock and SDS decellularized muscle scaffolds. Native muscle tissue (Fig. 2(A)) showed highly organized and repetitive sarcomeres, which were less pronounced in osmotic shock-treated muscle (Fig. 2(B)) and virtually absent in SDS decellularized muscle (Fig. 2(C)). Despite the remaining sarcomeric structure in osmotic shock-treated muscle samples, their myofibrils were out-of-register, leading to a disrupted myofibrillar arrangement. In contrast, when muscle tissue was decellularized with 0.1% SDS for 72 h, its sarcomere structure was profoundly absent.

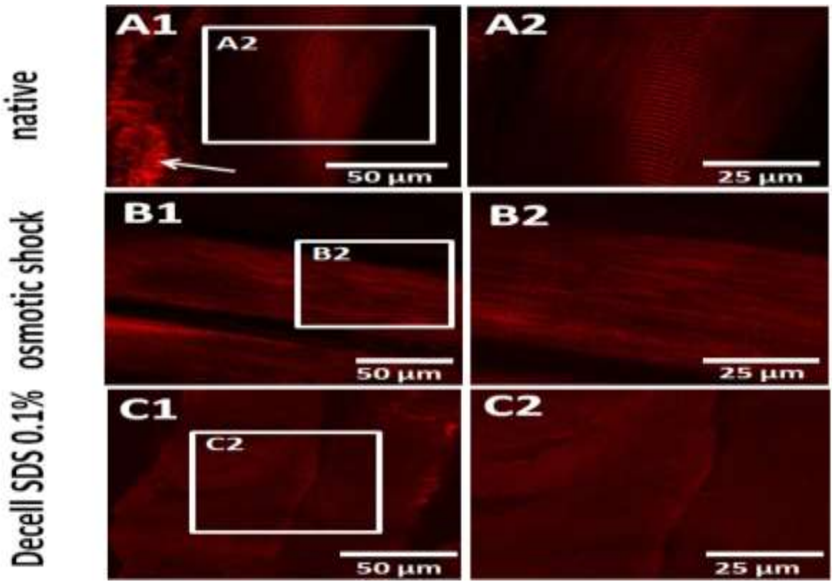

Fig. 2.SHG imaging confirms the absence of sarcomeres in M. gastrocnemius medialis after 72 h of 0.1% SDS perfusion-decellularization, while osmotic shock does not remove myofibrillar lattice components.

(a) shows representative SHG images of a native M. gastrocnemius medialis single muscle fiber within the muscle with a highly organized sarcomere striation pattern. Closely entwined collagen-I fibers are marked with an arrow. (b) Osmotic shock, induced with ultrapure water in whole muscles, only caused swelling of cells and disrupted the regular arrangement of sarcomeres but preserved their SHG signal. (c) In contrast, sarcomere structure entirely vanished after three days of dual perfusion-decellularization with 0.1% SDS in ddH2 O water and was, except for minor protein residues, undetectable even at higher magnification, confirming successful decellularization.

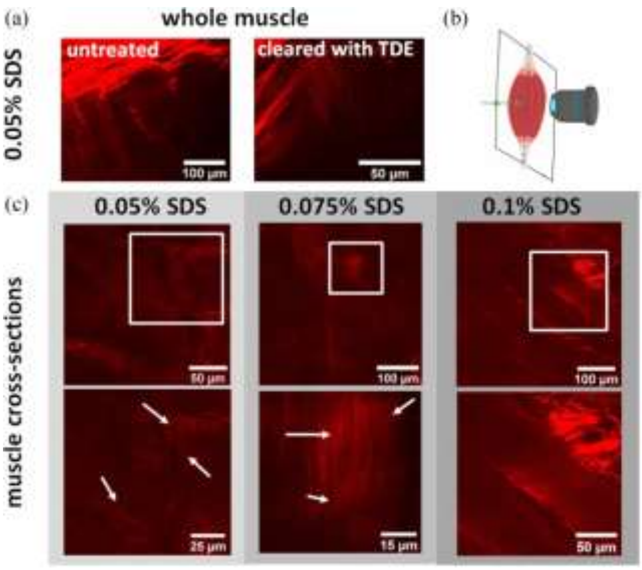

Fig. 3.SDS concentrations below 0.1% result in incomplete perfusiondecellularization within deeper tissue layers (~8 mm).

(a) SHG signals of muscles treated with 0.05% SDS, imaged through whole muscle and optically cleared muscle, respectively. (b) For all samples shown here, we imaged the longitudinal cross-section with two photon microscopy of optically cleared samples. (c) After decellularization with 0.05% SDS, few intact sarcomeres remained visible within the deep tissue (arrows). When using 0.075% SDS, the sarcomere pattern still persisted after 72 h decellularization. Eventually, at 0.1% SDS, the decellularization protocol entirely cleared the tissue of cellular components.

C. Microscopy Cross-Validation Confirms Protein Absence in Deep-Tissue Layers

To further confirm the quality of decellularized tissue, also (i) cross-validation with DAPI staining in combination with SHG myosin II imaging and (ii) scanning electron microscopy (SEM) was performed (Fig. 4 A & B). Both techniques independently show a loss of the muscle's native acto-myosin sarcomere structure, as well as the absence of cellular nuclei, and consequently align with our initial multiphoton-microscopy analysis.

D. Mechanical Stimulation Preserves Decellularization Quality

Another crucial quality parameter for successful decellularization is the quantity of remaining DNA per mg dry tissue (Fig. 4 C & D). A comparison between native and mere diffusiondecellularized tissue confirmed the latter to be inadequate for solid organ decellularization. Both samples did not differ significantly, neither when distinguished by probing surface- or deep tissue areas (Fig. 4 C), nor when comparing samples of different origin (Figure 4 D, native: ~ 150 ng mg−1; diffusiondecellularized: ~ 140 ng mg−1).

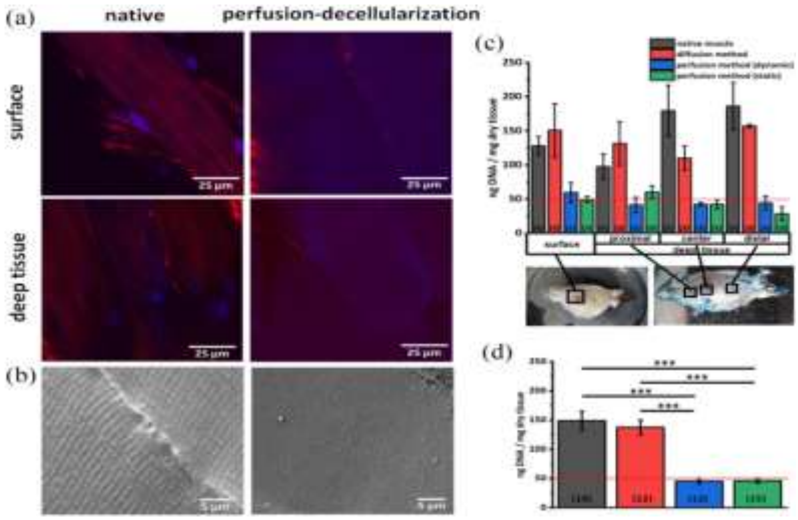

Fig. 4.Assessment of perfusion-decellularization quality confirms the loss of acto-myosin sarcomere structure. (a) SHG images comparing native to perfusion-decellularized muscle tissue after DAPI staining reveal a loss of sarcomere structure. (b) Electron-microscopy images of sarcomere ultra-structure show disorganization or vanishing of the native regular sarcomere pattern after decellularization. (c) DNA quantification of native, diffusion- and perfusion-decellularized muscle tissue extracted from the surface and

deeper tissue. Regardless of whether using dynamic stretching or no stretch at all (static), perfusiondecellularization, in contrast to mere diffusion, thoroughly clears the whole muscle of its cellular content and falls below a limit of 50 ng DNA per 1 mg dry tissue. Numbers in round brackets correspond to the total sample size. (d) Combining surface and deep tissue samples statistically confirms the effectiveness of perfusion-decellularization. (*: p <0.001).**

Biomechanical Characterization Indicates a Reduction in Passive Axial Elasticity in ECM Scaffolds

Since we confirmed that mechanical actuation does not impede on the final scaffold quality (no difference in remaining DNA content detected), this indicated that we could implement online passive elasticity assessment in our automated MyoBiodecellularization protocol without inducing stretch-induced artifacts to the decellularization process. This allowed us to track the muscle’s passive axial elasticity in resting-length tension (RLT) force-strain curves.

V. CONCLUSION

Our engineered MyoBio bioreactor system represents a resourceful advancement towards the automated production of skeletal muscle scaffolds for recellularization or reconstructive surgery. Due to its design, it can be applied to various different organs and tissue segments. While we chose a dual perfusion system, the set-up is easily modified into a multi-perfusion bioreactor system. Our automated perfusion-decellularization technique, involving 0.1% SDS, was confirmed to reliably decellularize even deep tissue layers of solid muscle organ and met the quantitative requirements to produce virtually cell-free ECM scaffolds (DNA content ≤50 ng mg^{-1}). Since we confirmed mechanical stimulation to not negatively affect decellularization quality, this provided us with the ability to assess the scaffold’s passive elasticity in RLT curves online, which will advance to a new process parameter to automatically report the decellularization progress on-the-fly.

References:

[1] J. Liu, D. Saul, K. O. Böker, J. Ernst, W. Lehman, and A. F. Schilling, “Current methods for skeletal muscle tissue repair and regeneration,” BioMed Res. Int., vol. 2018, 2018, Art. no. 1984879.

[2] C.-H. Lin et al., “Free functioning muscle transfer for lower extremityposttraumatic composite structure and functional defect,” Plast. Reconstructive Surg., vol. 119, no. 7, pp. 2118–2126, 2007.

Technology Innovation Continues to Drive Aerospace Electronic Systems Development

Student Name: Ms. AshwiniGhavale.

Class:TY Electrical Engineering

INTRODUCTION

TheIEEEAerospaceandElectronicSystemsSociety(AESS) encompasses technical fields of system design forlarge aerospace systems, radio frequency, and electronicsensors, instrumentation and fusion of multiple subsystems.Thesesubsystemsareintegratedwithelectronicdevices and signal processingto provide capabilities inradar, navigationandguidance, spacesystems, andmannedandunmannedvehicleswithcommunications interfaces. This Society has significant breadth for attractingsystems,sensors,andsignalprocessingresearchers. In the early 1960s, there were developments in military and civilian aviation, particularly with the increaseduseofsolid-statedigitalsystems.Space, military,andcivilian aviation came together in the growth of a tremendous aerospace industry with close ties to both NASA andtheU.S.DepartmentofDefense.

A small group of aerospace leaders from the Instituteof Radio Engineers (IRE)convenedtounderstandthetechnologicalissueslearned fromWorld WarIIaerialwarfare.AsH.WarrenCooperstated,

They were developing new systems’ capabilities with advanced aircraft, sensors, and communications techniques. In other words, a radar system makes use of microwave theory and techniques, antennas and propagations, electron devices, and ultrasonic ferroelectric and frequency control. All of these technologies go into the system. That started the new Aerospace and Electronic Systems Society to develop conferences, publications, and standards for new capabilities.As a result of this study, the AES Society was formed on 15 January 1973and projection of a historical trend

Figure1. Satellite constellation for aerospace vehicle position, navigation, andtiming[3].

However, the developments of solid-state physics and circuity

have maintained this capability for not only digital electronics but microwave monolithic circuits for the past 60 years. These technology advances helped propel new applications in space and airborne platforms, adaptive and electronically steered antennas, and high-speed signal processing. The new systems' capabilities will be illustrated in the following sections.

SPACE AND AIRBORNE PLATFORMS

The Global Positioning System (GPS) was one of the early aerospace systems developed to provide the position of military sensing platforms and eventually civilian use, over a high percentage of the Earth. The constellation of GPS satellites, shown in Figure 1, provides accuracy within 10 m worldwide. When combined with an onboard inertial navigation system (INS), the platform has an accurate capability for position, velocity, orientation, and time. This technology has enabled sensingplatforms to be independent of expensive and bulky navigation subsystems, which were originally required on all airborne surveillance platforms.Satellite sensing includes radars, electro-optical imaging, communications relays, and direct broadcast signals for television and entertainment. Based on many significant advances in sensor components and space qualified signal processing, a small constellations of satellites can provide accurate update on earth surface radar imaging. Similar microsatellites, as illustrated in Figure 2, will pro- vide wideband datalinks for providing telecommunications and data links to remote regions [4.Modern platforms for high altitude long-endurance (HALE) air vehicles, such as shown in Figure 3, provide a persistent imaging and communications platform in remote regions [5]. The evolution of composite materials and onboard electro-optical and radar sensors provided long range sensing of Earth surface features using syn- thetic aperture radar (SAR), ground moving target indica- tion (GMTI) modes, and interferometric radar (InSAR) for terrain height and land use features.

AIRBORNE RF SENSORS: Modern radio frequency (RF) subsystems for radar, elec- tronic support, and communications systems have become more capable with early technology from coherent solid- state transmitters and receivers. An important

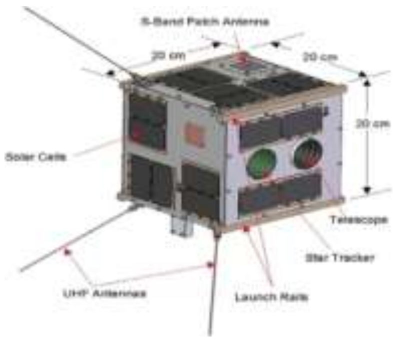

aerospace

Figure 2.Nanosatellite bus configuration

Figure3.HALE unmanned air vehicle

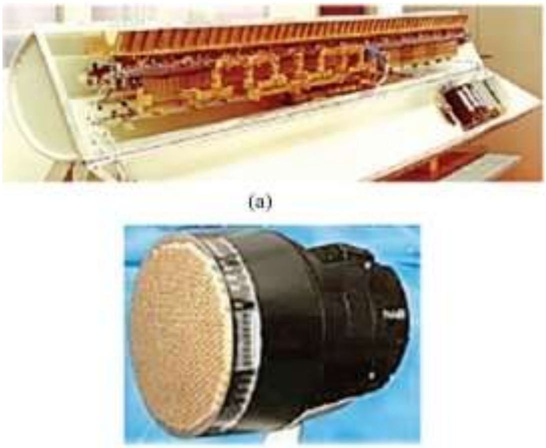

(a)

(b)

Figure 4.Phased array technology comparisons.

(a) Passive array ca. 1977. (b) Active ESA ca. 2007.subsystem was the electronically scanned antenna (ESA).This technology provided the ability to search a large vol-ume, without having mechanical scanning. A comparison of two ESA techniques is shown in Figure 4. The first early application was a passive ESA, employing analog phase shifters in the RF waveguide feed system and the more modern subsystem is an active ESA (AESA), which employs solid-state transmit and receive technology at each element.

A representative passive ESA system, illustrated in Figure 4(a), was constructed using a combination of RF waveguide and analog phase shifters to provide the elec- tronic antenna control [6]. With analog control after the transmitter and in front to the receiver elements, the two- way loss in signal provides a very inefficient radar opera- tion. Conversely, the AESA shown in Figure 4(b) has a small transmit-receive module immediately behind each of the radiating elements [7]. This architecture has very efficient RF operation, and significantly lower size, weight, and power.

Microwave integrated circuits (MIC) were readily available for early radar, RF sensing, and communications design and implementation. The design tools and imple- mentation had been developed for airborne avionics in the 1970s. However, the size and cost of these systems were limiting air and space applications. A significant advance in RF technology occurred in the late 1980s, where the RF chains could be implemented in a small number of mono- lithic microwave integrated circuits (MMIC) devices [8].

The comparison of these RF technologies is shown in Figure 5. The MIC technology in Figure 5(a) shows indi- vidual hybrid devices and controls on an integrated assem- bly [9]. Figure 5(b) shows a small number of MMIC chips integrating of transmitter low power chain and the whole receive chain implemented [8]. With the reduction of the assembly costs and the reduced size, weight, and power (SWAP), AESA designs were developed for many air- borne RF applications. Moreover, since the chips were significantly smaller than the MIC circuits, the depth of the AESA was reduced to a few 10s of centimeters. The TR modules are now feasible within a half wavelength square area behind the radiating face.

It should be noted that the greatest advances in solid-state transmitter components for RF sensing have come from the communications world. The production volume of devices for cell phones, cellular communications, and wideband signal modulation for spectrum conservation have reduced the production costs and increased utility of RF solid-state, active electronic scanned antennas.

HIGH-SPEED DIGITAL SIGNAL PROCESSING

High-speed digital signal processing has been a major enabling impact on aerospace systems. Early analog-to-digital converters (ADC) in coherent RF systems have pro- vided modest bandwidth and dynamic range for digital sig- nal processing. But due to their large size and complexity, only a small number of channels could be designed into the airborne and space systems. Based on the commercial needs for wideband communications, the high speed and dynamic range of ADC have been extensively improved.

The very high speed integrated circuit (VHSIC) Pro- gram was a U.S. Department of Defense research program that ran from 1980 to 1990 [10]. The benefits of this pro- gram were rapidly used in both military and civilian applications. More thanUS$1 billion in total was spent in the 1980s on the VHSIC program for silicon integrated circuit technology and applications

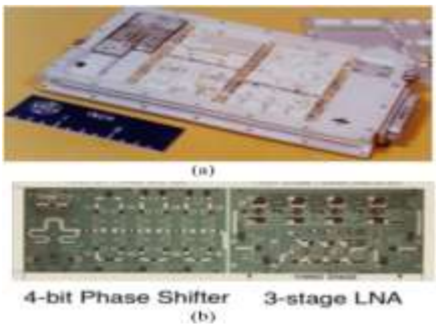

development.

Figure 5.Microwave integrated circuits for radar applications. (a) Micro- wave integrated circuit for AESA [9]. (b) Monolithic microwave integrated circuit for AESA [8].

One of the most pervasive technology advances has been the signal processing architectures with more speed and data intensive algorithms. These high-performance algorithmictools enabled radar onboard processing for real- time detection and characterization of the scene and objects within the images. The extension of Moore’s Law has been a combination of computational architectures and signal processing algorithms.

For onboard radar signal processing with increased resolution in synthetic aperture radar (SAR) and ground moving target indication (GMTI) sensing, the number of real-time floating-point operations per second (FLOPS) has continued to increase. Two examples of commercial off-the-shelf processing are given below. In 2001, a high- performance SAR signals processor to detect and a charac- terize small target under trees was demonstrated, as shown in Figure 6(a). Whereas in 2016, a single board FPGA processor could provide multiple mode, real-time processing, as shown in Figure 6(b). These two examples had comparable processing throughput, but with a reduc- tion of three hundred-to-one in size and cost [11].The culmination of these advanced technologies hasprovidedthe capabilities for ultimode systems on air craft andsatellites, with both small size andaffordable costs for distributed sensors on drones.

FUTURE TECHNOLOGIES FOR AES APPLICATIONS

The examples of system applications for RF sensing are a small portion of the Aerospace Electronics System Society technology portfolio, which have transitioned from experiments to operational development and production. The Society has produced conferences and publications for advancing technology in navigation systems, radar systems, instrumentation and measurement systems, cyber security, and fusion systems [12]. All of the capabilities over the past 50 years have benefited by the reduction in size, weight, and power for the hardware systems, direct digital RF synthesis, and increases in the digital computa- tion software for real-time applications. This section will briefly consider emerging technologies for the next decades.

FUTURE PLATFORM ARCHITECTURES

Small UAVs or drones have been developed for both military and civilian applications. A swarm of these platforms, shown in Figure 7, have been utilized for searching and characterizing objects of interest in diverse environments. The coordinated flying of these platforms utilizes global navigation satellite systems awareness, and network communication between drones for understanding and exploiting the scenario. Artificial intelligence between the platforms have been demonstrated in autonomous

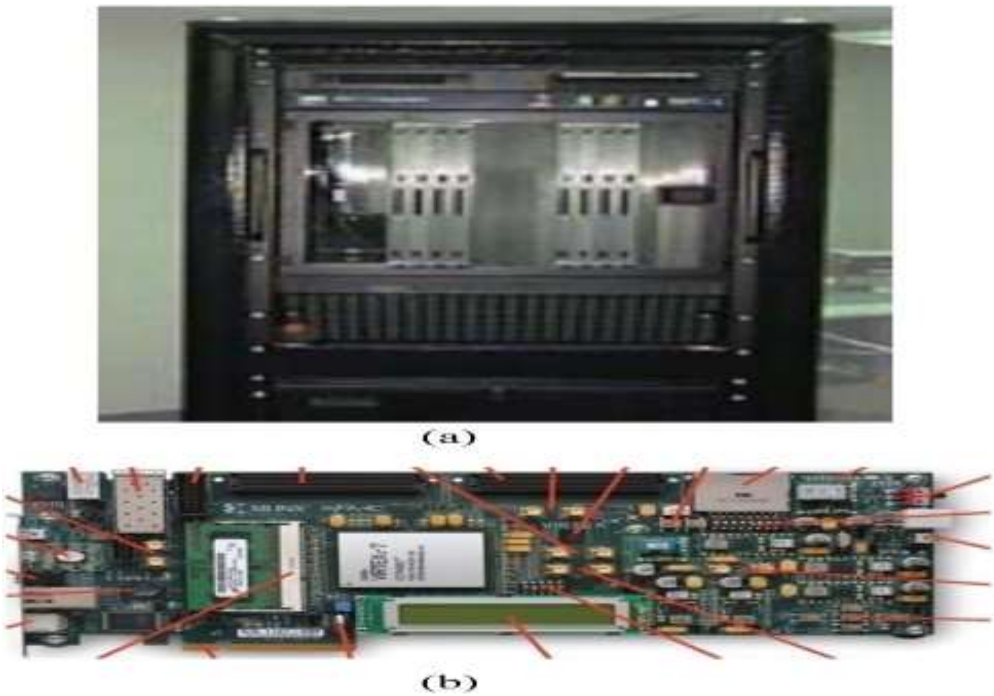

Figure 6.High performance computer comparisons [11]. (a) High performance multiprocessor. (b) Single board multicellprocessor.operation. Machine learning from the sensor inputs pro- vide characterization of the moving or stationary objects in the environment and scene [13].

MULTISENSING ARCHITECTURES

MMIC devices have extended their frequency and chip density to enable single-chip radars and RF receivers. The advent of the personal communications devices has extended the signals to millimeter wave frequencies. As a result, all smart phones have the ability to dynamically receive and transmit information globally.

Figure 7.
Swarm of small quad copters for surveillance [13].

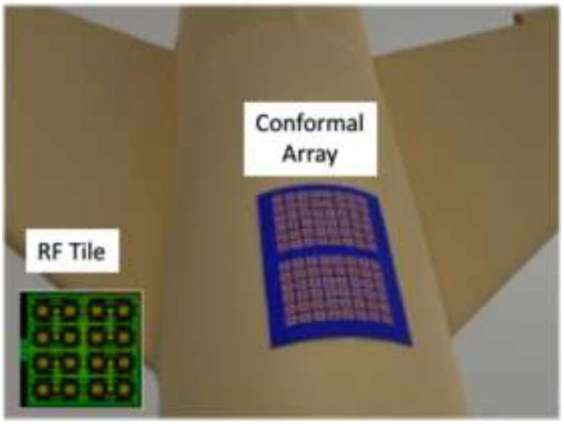

Figure 8.
Smart skin phased array for 5G communications [15].

being applied to sensing devices on small air vehicles (or drones) for networked surveillance within a geographic region. These technologies are being introduced in a significant number of commercial applications for monitoring remote regions and characterizing the environment for protecting our carbon footprint.

With the advent of systems on a chip and ultrawide- band waveform synthesis, multistatic and bistatic systems have significantly increased in importance for both long- and short-range surveillance [14]. With direct broadcast television from both space and on the Earth's surface, a source of RF illumination has provided persistent radar surveillance of aircraft and missiles for military defense applications. As multiple drones become more mature, and with very low receiver and signal processing, short range surveillance for border security and monitoring of commercial regions have been implemented.Smart skins for lightweight conformal arrays have been reported from the continued development in MMIC devices and high frequency/bandwidth devices have revolutionary applications to wide variety of platforms including small drones. The recent development of thin, smart skin phased array antennas has been implemented for aircraft radars and 5G communications [15]. Figure 8 illustrates the smart skin TR modules and a concept of phased array on the skin of an aircraft. These smart skin RF assemblies have been developed for "wearable" antennas, and application to small UAVs for networking within the swarms.

ARTIFICIAL INTELLIGENCE PROCESSING:Another rapidly developing research is Machine Learning where sensing and characterizing signals for communications, RF sensing of the background interference, and multi- mode resource operations are possible in a severely reduced RF spectrum. The areas of Machine Learning and Deep Learning have been widely publicized for improving aero- space applications. Reinforcement Learning is the problem faced by a computational agent to learn behavior through trial and error within a dynamic environment. The combination of Machine Learning with limited environmental propagation and interference data will provide continued improvement in adapting to the dense RF environment [16].

SENSOR FUSION

Multistatic sensing nodes have been considered for several decades. This is particularly important when the platforms are distributed in the area, as illustrated in Figure 7. Depending on the number of platforms, the digital data collection is needed on each platform for detecting or correlating the signal returns. These sensor designs will require wideband equalization of the individual channels in order to achieve the correlation metric between these sensors and the multiple channels on the sensor platform. Very wideband ADC and DAC devices are needed to pro- vide the amplitude and phase correlation for effective sensor fusion [17].Once a signal is sufficiently strong compared to thenoise or background clutter, the results are communicated to the other nodes for fusion. This is referred to a distributed fusion architecture. However, if the sensor requires more channels to separate the target from the background, the signal must be passed to a central fusion cell to provide the coherent processing objective.If there is a requirement for a large number of digital channels (Nch), the processing must be paralleled between a number of nodes (Ns). Depending on the required resolution of the sensing node, the sensor bandwidth will drive both the signal processing throughput and the communications bandwidth between the nodes or platforms. A simple example for the central data fusion is shown in Figure 9; where the total requirement of real-time processing is seen to grow significantly by the complexity of the system characteristics. The example shows several Teraflops (109.floating point operations per second) as an aggregate proc- essing in the multistatic architecture. This illustrates the continued need for the development of high-speed real-time processing, along with maintaining the bandwidth between the processing nodes [11].

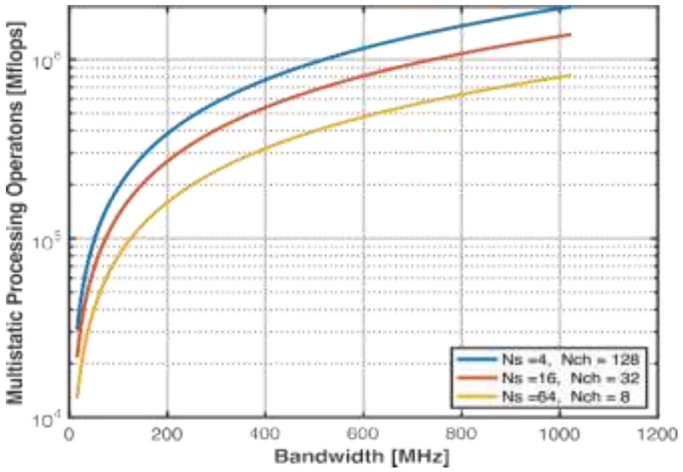

Figure 9.

Signal processing requirements for data fusion [11].

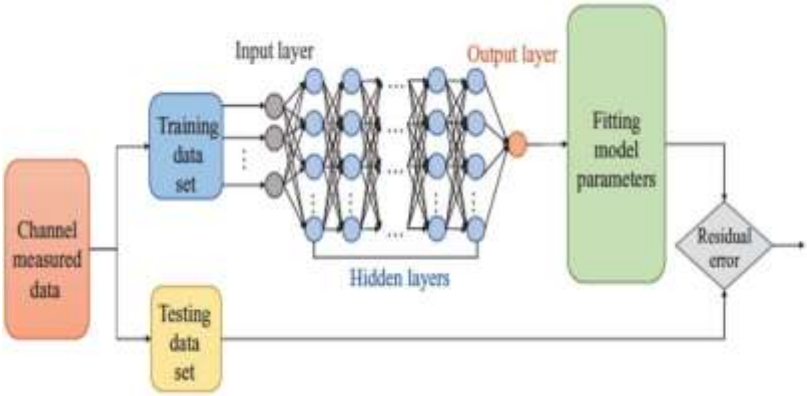

Figure 10.

Deep learning for RF channel modeling [21].

The continued technology development will require the communications architectures between sensors and processing nodes, in combination with advancing the Gig- aflops per watt in the onboard processing. Moreover, the most innovative technology advance is the prospect of quantum computing. There are several decades of improved processing speed to enable adaptive processing as well as secure linkage between multiple platforms. When the size of these devices is practical for airborne applications, the gap between VHSIC technology and future secure computing will be achieved [18].

SMART CITIES APPLICATIONS

There has been a significant thrust under the technology idea of Smart Cities, where information and communications are made available for people and businesses to manage their data in real time and to make better decisions. There is a pro- tocol evolving that will provide the internet to maintain the awareness for more efficient smart cities utilities. These util- ities will include power and connected and unconnected communications [19]. The technology drivers of the Internet of Things (IoT) include scalability, reliability, security, architecture, compliance, and standards. These drivers are similar to the aerospace systemschallenges, but on a larger scale due to the economic implications of IoT design and dissemination. AESS will need to follow and adopt many of the IoT standards and protocols to be affordable [20].

Over the past decade, the use of the RF spectrum has limited the ability for RF sensors and communications to coexist. The internet has been growing exponentially due to eCommerce, which in turn requires more RF band- width. The co-channel occupation between radars and civilian communications has been a significant challenge. There is a major benefit for applying deep learning to model the dynamic frequency allocation to avoid interference. Figure 10 illustrates an approach for 5G interference dynamic control. The advances in real time, adaptive processing on small sensing and communications platforms will require continued advances of Moore’s Law [21].

CONCLUSION

The IEEE AES Society has fostered a rapid growth of technology through conferences, publications in AES Sys- tems Magazine, and the Transactions in Aerospace and Electronic Systems, along with a series of Tutorials and Distinguished Lectures. The Society is multinational, with AES chapters in all 10 of the IEEE regions. This very pro- ductive networking has fostered the IEEE moto of "Advancing Technology for Humanity." We feel that the Society will continue developing these technologies via collaborative development with universities and industry.

References:

[1] "IEEE Aerospace and Electronic Systems Society history," Engineering and Technology History Wiki, Jul. 2014. [Online]. Available: https://ethw.org/IEEE_Aerospace_ and_Electronic_Systems_Society_History

[2] G. E. Moore, "Cramming more components onto inte- grated circuits," Intel Corporation, Electron., vol. 38, 1965, Art.no. 8.

[3] W. Thornton, "What's the difference between GNSS and GPS?," Jul. 2021. [Online]. Available: https://www.spirent. com/blogs/what-is-thedifference-between-gnss-and-gps

A Survey of FPGA-Based Vision Systems ForAutonomous Cars

Student Name: Ms.ShrutiJamdar

Class: SY Electrical Engineering

ABSTRACT :

On the road to making self-driving cars a reality, academic and industrial researchers areworking hard to continue to increase safety while meeting technical and regulatory constraints Understandingthe surrounding environment is a fundamental task in self-driving cars. It requires combining complex computer vision algorithms. Although state-of-the-art algorithms achieve good accuracy, their implementationsoften require powerful computing platforms with high power consumption. In some cases, the processingspeed does not meet real-time constraints. FPGA platforms are often used to implement a category oflatency-critical algorithms that demand maximum performance and energy efficiency. Since self-drivingcar computer vision functions fall into this category, one could expect to see a wide adoption of FPGAsin autonomous cars. In this paper, we survey the computer vision FPGA-based works from the literaturetargeting automotive applications over the last decade. Based on the survey, we identify the strengths andweaknesses of FPGAs in this domain and future research opportunities and challenges.

INDEX TERMS: Autonomous automobile, computer vision, field programmable gate arrays, reconfigurablearchitectures.

I. INTRODUCTION

Safety is always the most important concern for the humanbeings who interact on the roads as drivers, bikers, cyclists,or pedestrians. Most traffic accidents are caused by drivers.To reduce them, governments have strengthened legislationby introducing measures such as speed limits, breathalyzertests, airbags, etc. Despite the exceptional reduction of fatalities during 2020 due to the pandemic, there is a background trend towards an increase in the number of accidents.According to the World Health Organization, 1.35 milliondied on the road in 2016. One of the solutions to addressthis problem is the adoption of Advanced Driving AssistanceSystems (ADAS) technologies.

Self-driving functions can be implemented in several computing platforms such as ASICs, CPUs, DSPs, GPUs, FPGAs,or in heterogeneous platforms composed by any combinationof aforementioned platforms. One of the most distinct capabilities of FPGAs is that concurrent tasks can be parallelizedto a great extent by using techniques such as hardware partitioning or hardware pipelining. Moreover, the latency of someFPGA-based designs can be deterministic, which isoften a requirement for the car’s control system, especiallyfor safety-critical functions. As depicted in 2, FPGAs aretypically more energy efficient than other platforms exceptfor ASICs, which usually have higher Non-Recurring Engineering (NRE) costs. However, they provide higher flexibility and a significant lower time-to-market. Other platforms such as CPUs, GPUS, and DSPs provide higher flexibilitythanks to a more intensive use of external memory to storeintermediate results. This is also the main driver of theirgenerally higher energy consumption. For neural networkinference accelerators, FPGA implementations can be up to10× more energy efficient than GPU ones.

Our survey has specific comparisons on key performance metrics among various state-of-the-art implementations of ADAS problems, such as object detection, pedestriand detection, lane detection, and traffic sign recognition. Thecontribution of this paper includes:

• An analysis of vision-based problems on autonomouscars, key approaches and challenges.

• A survey of state-of-the-art FPGA-based implementations in the last ten years for those problems and gapindications.

• And a detailed exploration of the basic algorithmsor techniques that are used in the FPGAs-basedimplementations.

II. OVERVIEW OF FPGA TECHNOLOGY

After their humble beginnings serving as glue logic to connectthe important chips on a PCB, nowadays, FPGAs are considered full-fledged computing platforms and a valid alternativeto be used in high-end cars despite of their high cost The spatial computing paradigm can take profit of FPGAarchitectures for many highly parallel applications that havean important dataflow component, or high memory locality. Not all applications can benefit from full FPGA implementations, but even in many of these cases, FPGAs canstill offer some advantages whenused in conjunction withhost CPUs as accelerators. The speedup provided by suchaccelerators is often limited by the sequential part of thealgorithms running in the CPU as formalized by the Amdahl’slaw.Transistor density is a determinant factor of the performance and energy efficiency achieved in FPGA design. FPGA manufacturers have historically been early adoptersof new foundry nodes, therefore, benefiting from their latest advances in higher transistor densities and lower powerconsumption and following the Moore’s Law.

III. COMPUTER VISION SYSTEMS FOR AUTONOMOUS

CARSCV systems process data acquired from image sensors.In CMOS imagers, the electric charge induced by the lightirradiated over the pixel area is integrated by a capacitorduring the exposure time window. Imagers can be classified according to their acquisition process. In frame-basedsensors, output images are produced at a certain frequency. In event-based sensors, pixels are individuallyproduced as they reach certain requirements (such as reaching a light-integration threshold). The vast majority of CVresearch is based on frame-based sensors, although there isa growing interest in event-based CV algorithms Imagers can also be classified according to the wavelengthof the light they acquire. They can work in the visible andnon-visible wavelength ranges (infrared or X-ray). Consumer sensors typically work in the red, green, and blue visiblebands.

IV. BASIC ALGORITHMS

Many CV algorithms are based on basic image processing algorithms. These functional building blocks are oftenapplied to many pixels of the input images and can consume a relevant shareof total required computing power.Their ubiquity and performance requirements makes themgood candidates for FPGA implementations.

A. LOW-LEVEL ALGORITHMS

Many CV pipelines start processing the acquired images withalgorithms working at pixel level or small region level. Thoseare often considered low-level algorithms by their simplicityin terms of description. However, they might require highprocessing power as they are applied to many pixels.

B. FEATURE EXTRACTION

Feature extraction is the process that transforms input datain a more compact or meaningful representation so thatsubsequent processing steps can use them for detection orclassification. Feature extraction methods are often compute intensive and can be based on any combination of characteristics of the input images such as color, texture, shape, position,dominant edges, orientation, etc.

C. CLASSIFICATION

In some cases, classification is a final step in a recognitionalgorithm. There are some classification algorithms that havebeen implemented in FPGAs. Saidi conveniently surveysthem in. We will briefly describe some of them.Template matching is a simple classifier that works directlyon feature vectors. For each class c, we can have severalreference feature vector. As explained in section IV-A4,a similarity check against the reference vectors can be done toselect the reference class that gives the minimum difference.

D. NEURAL NETWORKS

Neural networks can work both for feature extraction andclassification. In fact, the boundary between both functionsis so thin that they are often perceived as a single block.Artificial Neural Networks, or simply Neural Networks(NNs), are bio-inspired circuits that try to mimic the functionof the neurons in the brain. The function of a neuronal layeri + 1 is often described by an activation function α on each
elementsof the result from the product between the inputvector xEi of layer i and a weight vector wEplus a bias BE.

V. THE CHALLENGES FOR FPGAs IN FUTURESELF-DRIVING CARS

In this section we will analyze the challenges that could faceFPGAs in the self-driving cars domain.

1) THE DEVELOPMENT EFFORT

Self-driving software stacks will require DL experts and software engineers with experience inmulti-processing systems.DL models are easily implemented into CPU and GPU platforms as many of the DL frameworks automatically considerthem as execution platforms. Therefore, there exist a gap between the ease of deployment between FPGA platformsand other platforms. We believe that a significant effortshould be devoted to reduce this gap and make it easierfor non-FPGAengineers to leverage the power of existingdevices.

2) TECHNOLOGY ADVANTAGE

The simple structure, regularity, and configuration facilitiesof FPGA devices used to be a good test for new foundrynodes, as so, they were usually using the latest available nodesafter the top market drivers (CPU manufacturers) and sometimes even before. However, market demand has increasedthe diversity of resources that now can be found in a FPGA,increasing their complexity. FPGA adoption of new foundrynodes is lagging behind of those for CPUs and GPUs forrecent nodes. It is specially relevant how fast TPUs haveembraced new nodes since the main challenges of self-drivingfunctions seem to comefrom the execution of DL models.The higher transistor densities given by new nodes are oftennot translated in smaller devices, but in higher transistorcounts for the same size and, in occasions, even in bigger devices. In FPGAs this translates into more resources,and with more available resources and bigger designs thecomplexity of place and route algorithms used synthesis isincremented, negatively affecting the design productivity.Also relevant, is that Xilinx has devoted their latest usedfoundry node to their new family of coarsegrain reconfigurable architectures (VERSAL).

3) COMPETING COMPUTING PLATFORMS

Future self-driving car systems will have several computing platform options to explore. There have beensome attemptsto analyze how several architectures(CPU/GPU/FPGA) can be part of on self-driving cars. However, the landscape is highly dynamic, and the analysis shouldbe revisited often until a clear option provides a significantadvantage. From our previous analysis, we estimate that anideal computing platform should be able to acquire data fromdifferent sensors in real-time, have a computingpower closeto 1 POPS, and an energy efficiency above 5 TOPS/W.Current mainstream multicore processors contain largevector units (e.g. implementing AVX512) that can be leveraged to execute NN models, but they are still far from the former performance and energy efficiency requirements. A newbreath of homogeneous many-core processors are addressing AI inference. A prominent example is the EsperantoET-SoC-1 that contains 1000 RISC-V cores. Pre-siliconestimations were claiming that it will be able to deliver morethan 100 TOPS within 20 W of power. This would resultin 5 TOPS/W.Tesla, who is already selling more than 1 million cars peryear, decided to develop its own FSD chip containing DPUs, which reaches 144 TOPS with a power consumption of 72 W,giving 2 TOPS/W. Tesladiscontinued using chips from NVIDIA and Mobil eye. Mobileye EyeQ5 reaches 24 TOPS,with a power consumption of 10 W, so 2.4 TOPS/W.Some DPUs are already above the 10 TFLOPS/W range. On GPUs, the recent NVIDIA RTX 4090 isproviding a significant computing power (82 fp16 TFLOPS),but at a highelectric power cost 800 W TPD. Using thesetheoretical values we would get an energy efficiency of0.125 TFLOPS/W According to Nvidia, the Drive Orin chip(optimized for automotive) is capable of 250 TOPS with apower consumption of 500 W, giving a 0.5 FLOPS/W.FPGA manufacturers are integrating highercomplexityblocks, actually transitioning from finegrain to coarsegrain reconfigurable architectures CGRAs. Xilinx VERSALdevices claim 160 (int8) TOPS at less than 180 W. This valueswould represent an energy efficiency of 1 TOPS/W. On theother hand, some FPGAs designsclaim 5.4 TOPS/W. Thesis the result of pushing down further the arithmetic precision.We actually see some convergence in DL architectures. Reduced arithmetic precision, SIMD architectures, andstrategies to increase memory locality and reduce externalaccess. If many competing platforms are achieving a similarperformance and energy efficiency range, then the dominancewill be the result of other aspects, like thedevelopment cost,support, and the development ecosystem.

VI. CONCLUSION

The paper captures the state of FPGA implementations forvision-based applications on self-driving cars for the lastdecade. The vision-based problems are presented and relatedto the typical functions ofautonomous cars. We identifyseveral key problems where FPGAs have been consideredas a valid implementing alternative: stereo-matching, semantic segmentation, lane detection, traffic sign recognition,traffic lights recognition, obstacle detection, and pedestriandetection. The state-of-the-art of each of them is analyzedto identify the approaches, challenges and basic techniquesbeing used in FPGA implementations. Published FPGAworks are listed and compared and their achieved accuracyand performance are put in context with respect their competing alternative computing platforms. Based on the survey,we provide the state-of-the-art achievements and we identifythe gaps for future research directions on FPGA-based accelerators for autonomous cars.

References:

[1] Y. J. Yasin, M. Grivna, and F. M. Abu-Zidan, ''Global impact ofCOVID-19 pandemic on road traffic collisions,'' World J. EmergencySurgery, vol. 16, no. 1, pp. 1–14, Dec. 2021.

[2] World Health Organization. (2018). Global Status Report on RoadSafety 2018: Summary (no. who/nmh/nvi/18.20). [Online]. Available:https://apps.who.int/iris/bitstream/handle/10665/277370/WHO-NMH-NVI-18.20-eng.pdf

A Network Intrusion Detection System for Building Automation and Control Systems

Student Name: Ms.AkshtaHiremath

Class: SY Electrical Engineering

ABSTRACT: Building Automation and Control Systems (BACS) are traditionally based on specialized communications protocols, such as KNX or BACnet, and dedicated sensing and actuating devices. Despite the increased awareness about the security risks associated with BACS, there is a lack of security tools for protecting this special breed of cyber-physical systems. This is further aggravated by the fact that general-purpose security tools are typically not able to cope with the specific requirements and technologies associated with BACS, making it necessary to devise domain-specific approaches – as shown, for instance, by the KNX Secure initiative led by the KNX Association. Nevertheless, despite the advances brought by KNX Secure and similar initiatives, there is still a considerable gap between the security needs of BACS and the solutions available. In this paper, we address this gap by proposing a Network Intrusion Detection System (NIDS) specifically designed for BACS. This NIDS is protocol-agnostic and can potentially support different BACS protocols and technologies, such as KNX, BACnet, Modbus or mixed ecosystems, without loss of generality. We also present a specific proof-of-concept implementation of this NIDS concept for KNX – one of the more widespread BACS protocols. To this purpose, a real-world KNX deployment was used to showcase and evaluate the proposed approach.

INDEX TERMS: Home automation, building automation and control systems, BACS, NIDS, smart buildings, security, safety, KNX.

I.INTRODUCTION

Over the past few years, there has been a progressive mindset shift in the automation domain towards considering security as much of a critical requirement as reliability or safety. From this perspective, Building Automation and Control Systems (BACS) constitute no exception, as both the need for monitoring the proper operation of physical devices and the security of the whole building operation should be considered as key requirements. This is especially important if one considers the increasing permeability between building automation and traditional IT systems, which increases the security challenges faced by BACS, since most of the current BACS implementations were originally designed with isolation as an acquired safety guarantee. The growing awareness of security problems led to various improvements to the standards used in building automation(e.g., KNX [1], BacNet[2] and ZigBee [3]),for instance incorporating authentication and encryption mechanisms. However, in most deployments it will not be easy or even possible to retrofit these improvements, since existing devices lack memory and/or computational power to implement those novel security features. Moreover, even buildings where these improvements are retrofitted are still vulnerable to a wide range of attacks.

I. II. KNX-BASED BACS

This section provides a basic description of the KNX protocol and related technology ecosystem. More detailed information can be found on the KNX Association repositories [4]. The KNX standard appeared in the early 1990s, driven by the European InstallationBus Association (EIBA [1]) as a way to enable the connection, configuration and communication between multiple building automation devices (e.g. sensors, actuators, buttons and other user interfaces), using a common language and a standard communications protocol. It is widely used for home and building automation, for instance to control lighting, shutters, security systems, energy management, heating, ventilation, air-conditioning systems, signaling and monitoring systems, remote control, and audio/video control. All these functions are managed via the KNX protocol set. Opposite to traditional electric installations, KNX installations have no dedicated hard-wired connections between control devices and actuating devices. For example, a light switch is not directly connected with the controlled lights. Instead, all devices are connected via a shared bus that runs on 29 Volt. All bus devices can be programmed with a common tool, enabling easy and flexible deployment. Moreover, subsequent changes require no rewiring.

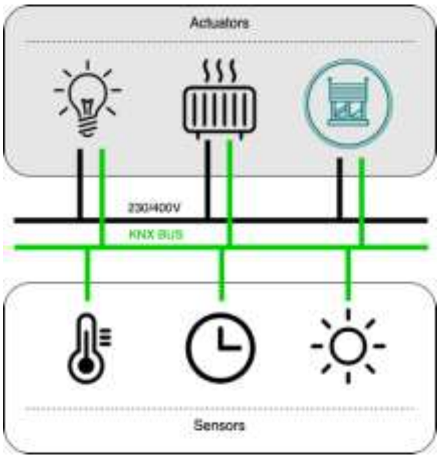

FIGURE 1. Basic KNX elements.

A KNX system requires the following components (cf. Figure 1):
FIGURE 1. Basic KNX elements.

- Power supplies that feed the bus and KNX devices.
- Sensors (push buttons, thermostats, air velocity meters, etc.) that generate commands as telegrams.
- Actuators (switch relays for lights, blinds, etc.) that receive the telegrams and perform predefined actions.
- The bus that connects all sensors and actuators.

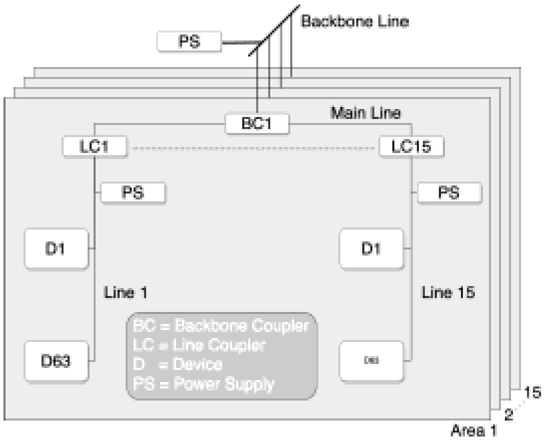

FIGURE 2. KNX logical topology

The development of KNX-certified devices can follow three different models: partial, OEM (Original Equipment Manufacturer) or full development. Partial development devices are based on available and already certified system components, communication stacks and modules, including the (KNX-certified) Application Program. OEM devices are straightforward relabels of already certified KNX devices (typically developed by other KNX members), with this option the development effort is reduced to nearly zero, and only the Application Programs need to be registered in the name of the reselling manufacturer. Lastly, fully developed devices require several steps: definition of the characteristics, selection of the profile, selection of the communication medium, implementation of the stack and, finally, the development of the Application Program. Then, the Application Program will be signed by the KNX association and certified using tests by certified entities. KNX is a fully distributed network, which accommodates up to 65,536 devices in a 16 bit Individual Address space (see Figure 2). The IA of each device is composed by its area, line and device numbers, in the format arealinedevice.

II. CYBERSECURITY AND BACS

Historically, BACS have been designed to work in an isolated fashion, without any connection to ICT networks. Security was supposedly achieved by isolation (the ''airgap principle'') and by the use of obscure proprietary solutions with poor or non-accessible documentation. Meanwhile, the popularity of ICT commodity technologies – driven by simplicity, lower total cost of ownership and improved operation, configuration and management – has led to the introduction of network bridging mechanisms. Suddenly, several underlying security assumptions were broken, and BACS became connected to globally accessible networks such as the Internet, without taking into account the potential implications in terms of security and safety. As pointed out by Graveto et al. [9], BACS security breaches are often considered to be a consequence of using systems, protocols and standards that were originally conceived to operate in isolated environments, without any connection to ICT networks or the Internet. This is aggravated by the fact that many legacy devices cannot be patched, often meaning that only isolation or complete replacement might ensure adequate security [10]. In general, most attack categories that are characteristic of Industrial Automation and Control Systems (IACS) may be somehow transposed to BACS scenarios [11]. However, even though some the protection strategies used in IACS might somehow provide hints on how to keep BACS secure, there are considerable context differences that require domain-specific approaches. Similarly, the protections typically used in IACS at network level also need to be adapted to BACS.

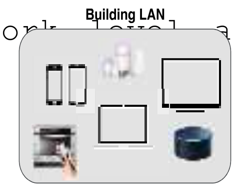

III. INTRUSION DETECTION FOR BACS SCENARIOS

As already discussed, several successful attacks have occurred and existing mechanisms were unable to detect them, pointing to the need of better intrusion detection systems for BACS. Actually, there is already extensive work in anomaly and intrusion detection in related areas, such as cyber-physical systems and IoT [17], [18], [19], [20], but there are much less proposals in the specific topic of building automation. Pedro and Silva [21] proposed the development of generic monitoring and actuation of home automation facilities for use with different technologies. This solution is based on the DomoBus technology, whose device abstraction model and communications service supposedly enable the development of configurable applications from XML (Extensible Markup Language) files – allowing for monitoring and control of device networks based on several technologies. Jones et al. [22] used a Single Board Computer (SBC) to deploy an unsupervised artificial neural network to monitor building automation systems. The proof-of-concept used BACnet and all the network packets were stored and analyzed using an on-board Adaptive Resonance Theory neural network. When anomalies are found, the source and destination addresses are added to an access control list and those communications are blocked. In our opinion, this type of automated reactions may become a problem for the overall performance of the building system, and even constitute anew attack vector to be exploited by malware – as already known in similar domains such as IACS. This could be solved by means of human intervention in the reaction process, for improved safety.

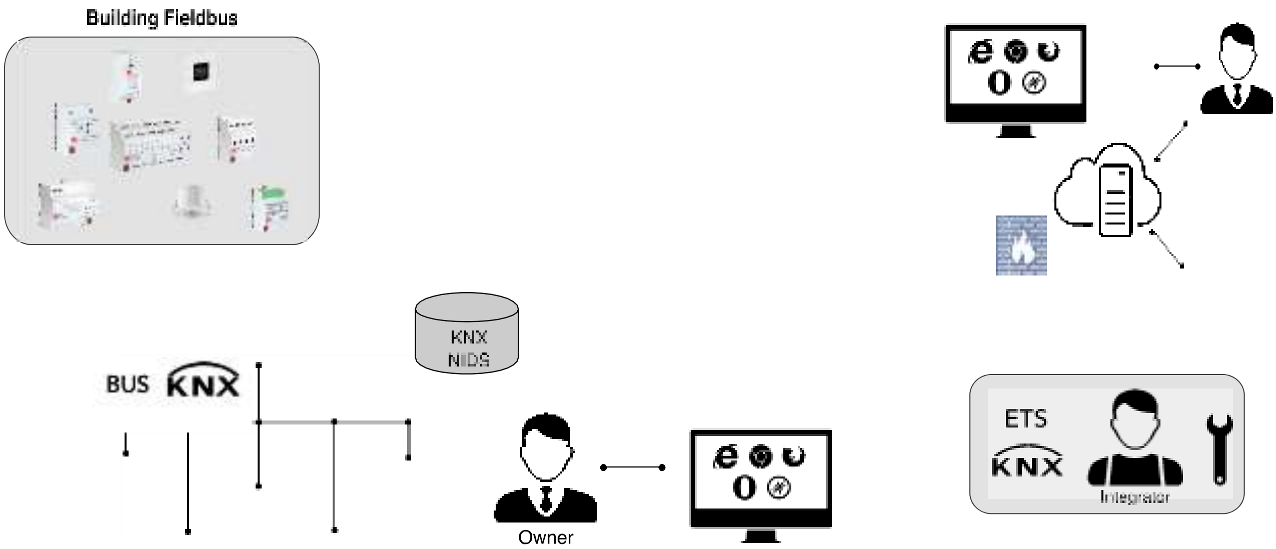

FIGURE 4.BACS Security Architecture.

IV. PROPOSED BACS NIDS

The discussion presented in the previous section clearly identified a gap of security mechanisms for BACS environments. This motivated us to develop the BACS NIDS, an intrusion and anomaly detector that operates mainly at the control network level (fieldbus). The concept and main requirements are outlined in this section, with the architecture being presented in Section VI.

FIGURE 5.BACS KNX NIDS Integration Model.

A. THE CONCEPT

The proposed integration model for the BACS NIDS is illustrated in Figure 5. It is built around an SBC with two interfaces, one connected to the building fieldbus (KNX twisted pair or other support medium) and an Ethernet interface connected to the local building LAN. The proposed approach is also compatible with other building automation standards (e.g. BACnet, ZigBee, EnOcean), despite KNX being the target protocol for the proof-of-concept implementation hereby presented. The BACS Security Management Platform constitutes a web application that can be either locally served by the KNX NIDS host or remotely exposed by a web server, using an outof-band ethernet connection. The security events generated by the system are forwarded to the platform, processed and presented in a friendly user interface (UI). This same UI may also provide management and configuration capabilities, supported by KNX NIDS management events.

B. REQUIREMENTS

The design of the BACS NIDS considers the following key principles:

• Seamless and transparent operation – by design, most of the
required evidence for processing should be obtained by passively monitoring the protocol message flow, without any interference in the normal operation of the BACS.

• Cost-effectiveness – the NIDS must be cost-effective when compared to regular automation devices, ideally being within the same price range.

• Protocol readiness – The device should be fully compatible with the target BACS standards (e.g. KNX), for stealth operation and compatibility with existing BACS devices.

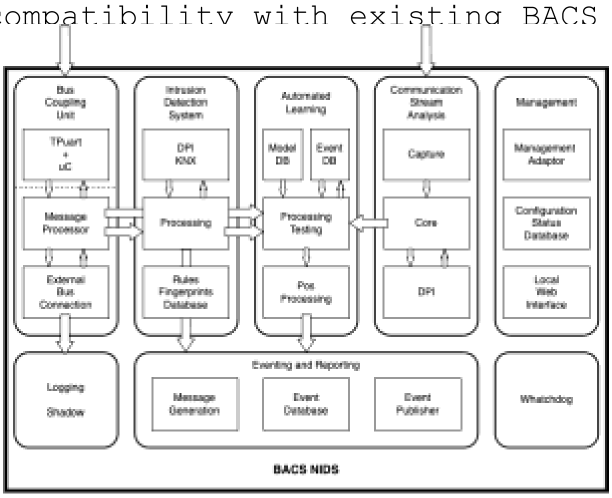

FIGURE 6. BACS NIDS Architecture.

V. PROOF-OF-CONCEPT IMPLEMENTATION

The architecture of the PoC NIDS is presented in Figure 6. It is based on a neutral concept that is compatible with the majority of BACS protocols (e.g. KNX, BACnet, Modbus), communications technologies (e.g. KNX TP, KNX RF, Ethernet, Zigbee, RS-485) and deployment scenarios. Nevertheless, for sake of readability, some of the technical details discussed

in the following subsections directly relate with the PoC prototype developed for BACS, which based on a KNX TP bus.
The remainder of this section discusses in more detail each of the main building blocks of the KNX NIDS architecture: bus coupling unit; intrusion detection system; automated learning; communications stream analysis; management; shadow logging module; eventing and reporting; and watchdog.

VI. CONCLUSION

Despite their relevance, from a security and privacy point of view, BACS ecosystems suffer from a lack of domain-specific security tools, since general-purpose tools are unable to fully address the requirements of such environments. To address this gap, in this paper we proposed a domain-specific NIDS designed for BACS environments, able to monitor and analyse fieldbus traffic and able to fit into typical BACS scenarios, in terms of physical deployment, costs and management interfaces.
After introducing the proposed concept, we described a specific PoC implementation for KNX TP fieldbus, discussing its software architecture, hardware details and generic detection and management capabilities. Afterwards, we demonstrated these capabilities in the scope of a real BACS scenario, injecting several types of attacks and using statistical analysis, signature-based rules and artificial intelligence techniques to detect those attacks.

Reference:

[1] J. C. Mace, C. Morisset, K. Pierce, C. Gamble, C. Maple, andJ. Fitzgerald, ‘‘A multi-modelling based approach to assessingthe security of smart buildings,’’ in Proc. Living Internet Things,CybersecurityIoT, 2018, pp. 1–10. [Online]. Available: https://digitallibrary.theiet.org/content/conferences/10.1049/cp.2018.0031

Quantum Information Science

Student Name: Ms.SameenaMakhmalla

Class: TY Electrical Engineering

ABSTRACT

Quantum computing is implicated as a next-generation solution to supplement traditional von Neumann architectures in an era of post-Moore's law computing. As classical computational infrastructure becomes more limited, quantum platforms offer expandability in terms of scale, energy consumption, and native 3-D problem modeling. Quantum information science is a multidisciplinary field drawing from physics, mathematics, computer science, and photonics. Quantum systems are expressed with the properties of superposition and entanglement, evolved indirectly with operators (ladder operators, master equations, neural operators, and quantum walks), and transmitted (via quantum teleportation) with entanglement generation, operator size manipulation, and error correction protocols. This article discusses emerging applications in quantum cryptography, quantum machine learning, quantum finance, quantum neuroscience, quantum networks, and quantum error correction.

INTRODUCTION

Quantum computing is the use of engineered quantum systems to perform computation, meaning physical systems comprised of quantum objects (atoms, ions, and photons) manipulated through configurations of logic gates. "Quantum" refers to the scale of atoms (nanometers 109), ions and photons (picometers 1012), and subatomic particles (femtometers 1015). The general expectation in quantum computing is a quadratic speedup in the computation of certain kinds of equations. Algorithms are being rewritten to take advantage of the quantum speedup in processing linear algebra routines, Fourier transforms, and other optimization tasks. The development of quantum technologies is a worldwide effort spanning several hardware platforms that are currently available via cloud services (e.g., IBM Q 27-qubit, IonQ 32-qubit, and Rigetti 19Q Acorn systems) and that have been announced in research efforts (Google’s 53-qubit Sycamore quantum processor). Contemporary quantum systems are nonerrorcorrected noisy intermediate-scale quantum (NISQ) devices constrained to 50–100 qubits. The millionqubit systems needed for full-scale quantum operations (such as Shor’s factoring algorithm and Grover’s search algorithm) are not immediately immanent. Technical breakthroughs are needed to deliver the quantum error correction required to progress from NISQ devices to fully fault-tolerant quantum computing (FTQC).1 However, progress in many areas of foundational physics is enabling new technologies that translate to practical use in quantum computing, for example, a black-hole-on-a-chip formulation and experimental setups for testing quantum gravity in the laboratory

QUANTUM CRYPTOGRAPHY

One of the most immediate high-profile applications of quantum computing is cryptography. The “Y2K of crypto” problem is that practical quantum computing will break the security of nearly all modern public-key cryptographic systems (based on SHA-256 and related hashing algorithms).3 Postquantum cryptographic algorithms that are resistant to quantum computerbased attacks will need to be implemented in a worldwide roll-out effort. The development of quantumresistant public-key cryptographic standards is underway, with the algorithm selection process expected to be completed by 2023. In June 2021, the U.S. National Institute of Standards and Technology (NIST) announced that their postquantum cryptography standardization process had entered the third phase, with seven third-round finalists and eight alternate candidates being considered for standardization. The mainstay application for postquantum cryptography is quantum key distribution on global networks. Quantum-secure algorithms mainly involve a shift to mathematics based on lattices (group theory) as opposed to factoring (number theory). Some of the first quantum algorithms developed to take advantage of nonclassical properties were Shor's quantum factoring algorithm and Grover's quantum search algorithm. Shor's algorithm is a period-finding function with a quantum Fourier transform (a classical discrete Fourier transform applied to the vector amplitudes of a quantum state), which is exponentially faster than classical algorithms (the general number field sieve). More recently proposed quantum-secure cryptographic methods include access based on location instead of authorization, with quantum secret sharing localized to space-time, and authorized regions replacing authorized parties. Time entanglement (entanglement in time instead of space) is also possible for cryptographic key exchange within a short time window

QUANTUM MACHINE LEARNING

Quantum machine learning (machine learning applied in a quantum environment) is emerging as one of the first potential general-purpose applications of nearterm quantum devices. A key advance is the Born machine as the quantum version of the Boltzmann machine.5 Both "machines" are automated energy functions that evaluate probability output from machine learning algorithms. Classically, the Boltzmann machine uses an energy-minimizing probability function for sampling (per the Boltzmann distribution in statistical mechanics). The Born machine interprets results with the Born rule (a computable quantum mechanical formulation that evaluates the probability density of finding a particle at a given point as being proportional to the square of the magnitude of the particle's wavefunction at that point).

QUANTUM FINANCE

Quantum finance is the application of physics methods to problems in finance, namely, option pricing, trading strategies, risk management, and portfolio optimization. Markets have long been modeled as complex physical phenomena per the principles of wavefunctions, thermality, dissipation, and Brownian motion, and now these models are being implemented with real-life quantum hardware instead of simulation. Quantum finance could be one of the first mainstream fields to develop in quantum computing as the financial industry is typically an early adopter of new technologies, and currently finds itself in a potential progression from classical to digital (blockchains) to quantum methods. So far, the main quantum algorithms deployed in finance include quantum amplitude estimation algorithms, quantum Monte Carlo methods, anvharmonic oscillators, and quantum kernel learning. Quantum amplitude estimation algorithms are used to estimate the properties of random distributions such as risk measures.11 A quantum circuit is defined with a unitary operator to act on a register of qubits and an estimation operator to operate on the system based on quantum phase estimation (approximating certain eigenvalues of the estimation operator). Qubits are put into superposition (by applying the Hadamard gates) and used to control different powers of the estimation operator. The system is evolved (by applying an inverse quantum Fourier transform) and the qubit state is measured. The result is an integer that is mapped to a classical estimation function. Streamlining the phase estimation process requires even fewer gates. Tested on the IBM Q 20-qubit Tokyo system, the method indicates a quadratic speedup compared to the convergence rate of classical Monte Carlo methods.

QUANTUM NEUROSCIENCE

Quantum neuroscience is the application of quantum information science methods to problems in neuroscience, particularly wave-based analysis, quantum biology state modeling, and neuroscience physics.13 Some of the first quantum neuroscience applications use quantum machine learning to study EEG data with quantum neural networks, for example, proposing a quantum circuit to extract 794 features from 21 EEG channels to evaluate Parkinson's disease patients for deep brain stimulation treatment. One research project has developed quantum algorithms to reconstruct medical images from MRI, CT, and PET scans (MRI images with an inverse Fourier transform, and CT and PET images with an inverse Radon transform and the Fourier slice theorem). Another project integrates EEG and fMRI wave-based data at various spatiotemporal scales and dynamics regimes. A key finding is that whereas epileptic seizure can be explained by chaotic neural dynamics, normal resting states are more complicated, and are perhaps explained by bifurcation neural dynamics, in which there is an orbit-based organizing parameter periodically interrupted by countersignals to trigger a neural signal. The second level of quantum neuroscience applications is quantum biology state modeling, which involves superpositioned data (the superpositionbased modeling of data as the quantum information representation of all possible system states simultaneously) and quantum probability.14 Biological systems constantly interact with their environment and change their behavior as a result. Models thus include updating processes in which the system takes measurements and responds accordingly. Quantum biological states are interpreted with quantum probability, quantum mechanical rules for assigning probabilities that accommodate interference effects that violate the law of total probability, and commutativity in conjunction, in classical systems. A quantum variant of total probability can be obtained with an interference term for incompatible observables given by positive operator-valued measures, positive measures on a quantum subsystem of the effect of a measurement performed on the larger system. The main interpretation of quantum probability is with the Born rule, but there can be others. Quantum Bayesian methods, notably QBism ("cubism"), incorporate subjective (observer-based) aspects.

QUANTUM NETWORKS

Global-scale quantum networks are envisioned for ultrafast, ultra-secure communication, computation, and sensing. Such networks would likely be photonic, relying on expertise in global fiber optic communications dating from the 1960s. A full-stack roadmap (analogous to the OSI stack) is proposed for end-toendqubit delivery and heralded entanglement.4 Entanglement generation is a central requirement for quantum networks (for quantum key distribution and quantum teleportation), and various plans outline distilled, swapped, heralded (confirmed), and high-dimensional entanglement.

QUANTUM ERROR CORRECTION

The central factor in the long-term feasibility of quantum computing is error correction.1 Error correction protects quantum information states from environmental noise. Noise arises in communications networks as quantum states pass through noisy channels, and in quantum computing as additional error classes are introduced in information processing.

Classical error correction methods, such as making redundant copies or checking information integrity before transmission are not possible in quantum systems since information cannot be copied or inspected (per the no-cloning and no-measurement principles of quantum mechanics). Quantum error correction therefore often relies on entanglement instead of redundancy. The quantum state to be protected is entangled with a larger group of states from which it can be corrected indirectly (one qubit might be entangled with a nine-qubitancilla of extra qubits).The standard errors are a bit flip, a sign flip (the sign of the phase), or both. Basic codes diagnose the error, corresponding to the Pauli matrices for controlling qubits in the X, Y, and Z dimensions. The error is expressed as a superposition of basis operations given by the Pauli matrices. If there is an error, the same Pauli operator is applied to act again on the corrupt qubit to reverse the error effect. The unitary correction returns the state to the initial state without measuring the qubit directly.

The basic form of the quantum error-correcting code is the stabilizer code (applied via ancilla), as the quantum version of linear codes used classically. In quantum computing, topology-based stabilizer codes (the toric code and the surface code) are proposed as a potential method for fault-tolerant error correction. Particle movement and its correction are interpreted in the structure of lattice topologies. Toric codes are stabilizer codes defined on a 2-D lattice with periodic boundary conditions (thus giving the shape of a torus), with stabilizer operators on the spins around each vertex and plaquette (face). Surface codes are a more generic formulation of topology-based stabilizer codes, which are also defined on 2-D spin lattices, and take various shapes, but are not necessarily toroidal. Lattice surgery is a method of switching between codes on the fly.

CONCLUSION

Quantum information science is a field with substantial progress and near-term opportunity, but also risks. It may be too early in the technology cycle if fault-tolerant error correction methods cannot be found and platforms do not progress beyond hundred-qubit systems. Sharper critiques are that more foundational quantum algorithms should have been discovered by now, that quantum problem-solving may be limited to certain kinds of operations (e.g., linear algebra), and that a fullblown quantum infrastructure (processors, repeaters, networks, and memory) is needed to assess the potential contribution of the technology. However, despite these challenges, it is not too early to reformulate classical problems for computing in the quantum domain and begin testing on quantum simulators and near-term quantum hardware available via cloud services. At minimum, quantum computing provides an alternative platform to ease the burden on classical von Neumann architectures in a moment of transitioning to post-Moore's law computational solutions. Overall, quantum computing emerges as a novel computational platform that provides a more capacious architecture with greater scalability and energy-efficiency than current methods of classical computing and supercomputing and more naturally corresponds to the 3-D structure of atomic reality.

Reference:

[1] A. R. Brown et al., "Quantum gravity in the lab: Teleportation by size and traversable wormholes," 2019, aXiv:1911.06314v1.

[2] W. Barker, M. Souppaya, and W. Newhouse, Migration to Post-Quantum Cryptography. Rockville, MD, USA: NIST Nat. Inst. Standards Technol. Nat. Cybersecurity Center Excellence, 2021, pp. 1–15.

A Light-Field Journey to Virtual Reality

Student Name: Mr.PravinKhatave

Class: B.Tech Electrical Engineering

With Facebook's acquisition of the VR startup Oculus in 2014 for approximately US$2 billion, VR reemerged from research laboratories better pre- pared for success in the public marketplace. Since then, other tech giants—including Micro- soft, Google, Sony, HTC, and Samsung—have released popular VR and augmented reality (AR) headsets—such as the Sony PlayStation VR (www.playstation.com) and HTC Vive—to provide fun and exciting experiences. Furthermore, smaller startup companies, such as 8i,Otoy, and Lytro, have started focusing on producing ultra-high- quality content, recognizing that this will be the next grand challenge in the VR industry.

Producing high-quality VR content is difficult, because our eyes are very good at distinguishing between what is and isn't real. For example, the binocular stereoscopy of human eyes is largely missing in traditional 360- degree panoramic video-capture solutions. More advanced imaging systems, such as ones equipped with depth cameras, can recover certain aspects of 3D geometry to generate stereoscopic pairs. However, partial 3D is still insufficient to provide motion parallax, which is essential for providing a realistic viewing experience. In addition to stereo and motion parallax, human eyes also achieve 3D vision through refocusing, where only the object in the focal plane is clear and objects at other distances are blurry. The real world presents extremely high-dimensional data, comprising geometry, lighting, surface reflectance, and so on. We must record every piece of information in this high-dimensional dataset to faith- fully reproduce reality.

Consequently, to create a virtual reality that even the human eye cannot distinguish from the real world, we must achieve the perfectimmersive viewing experience, such that human viewers feel they can walk into the scene. This is known as the virtual *walk-in effect,* and it requires *light-field technology*—3D imaging technology that emerged from the field of computational imaging/photography to capture the light rays that people perceive from different locations and directions. When combined with computer vision and machine learning, light- field technology provides a viable path for producing low-cost, high-quality VR content, positioning this technology to be the most profitable segment of the VR industry. In fact, as VR technology enters everyday life, the frontier of light-field VR will become increasingly attractive by emulating real 3D worlds, including complex objects, humans, and large environments

Human Visual Perception

VR has rapidly become popular because of its ability to create an immersive experience in which people can observe and feel the content. To achieve this, the virtual scene must be presented in the form of a 3D panoramic image or video, and the scene should change rapidly to accommodate human head motion. It should also provide sufficient depth information for the human eye and brain to determine the range of objects and simultaneously change focus.

Human beings acquire most of their information about the world through their eyes. Shaped by physiological evolution and extensive daily training, the human eye has cultivated an effectivemechanism to perceive the external world, and this mechanism of perception is ultra-sensitive. For example, the human eye is very sensitive to depth information, which is perceived through clues such as binocular parallax, motion parallax, occlusion, and convergence. More specifically, when people observe an object in the real world, their eyes are constantly changing focus and, via the vestibular reflex, the resulting jitter and blur are eliminated. The real world is visualized via numerous light rays, which the human eye captures from different locations and directions by changing its focus. With head motion, human eyes can always focus on the object of interest, even if the object is surrounded by a changing environment.

The collection of light rays that people perceive from different locations and directions in their surroundings is the light field.

Why Light Fields?

When wearing a VR headset, the human eye is actually focused on the viewing screen inside the headset, while the virtual reality is trying to "deceive" the human eye and brain, as if the eyes were focused at different depths. Once there is some error or delay in displaying the content, the human eye will be attuned to perceiving these artifacts, which subsequently could cause uncomfortable symptoms such as headaches, dizziness, or fatigue. In contrast, if human eyes can directly perceive the VR con- tent in the form of a light field, many of these visual discomforts would be significantly reduced if not completely eliminated.

In the past decade, researchers from both computer vision and computational photography have developed different means to record and reproduce the complete light field. The most notable examples are commodity light- field cameras, such as those from Lytro and Raytrix (www.raytrix.de), and light-field camera arrays,1,2 which enable easy acquisition of light fields at various scales. Besides imaging solutions, recent efforts have focused on applying light fields to resolve challenging problems in computer vision and robotics, including stereo matching and 3D reconstruction, stereoscopy synthesis, saliency detection, surveillance, and recognition. There has also been useful research in several geometrical aspects of light-field cam- eras, such as calibration. In 2014, my colleagues and I organized the first Light Field for Computer Vision (LF4CV) workshop, in conjunction with the European Conference on Computer Vision (ECCV 14) and a special issue on the topic in the journal, Computer Vision and Image Understanding.3 This year, we're organizing the second LF4CV workshop in conjunction with the conference on Computer Vision and Pattern Recognition (CVPR 17).

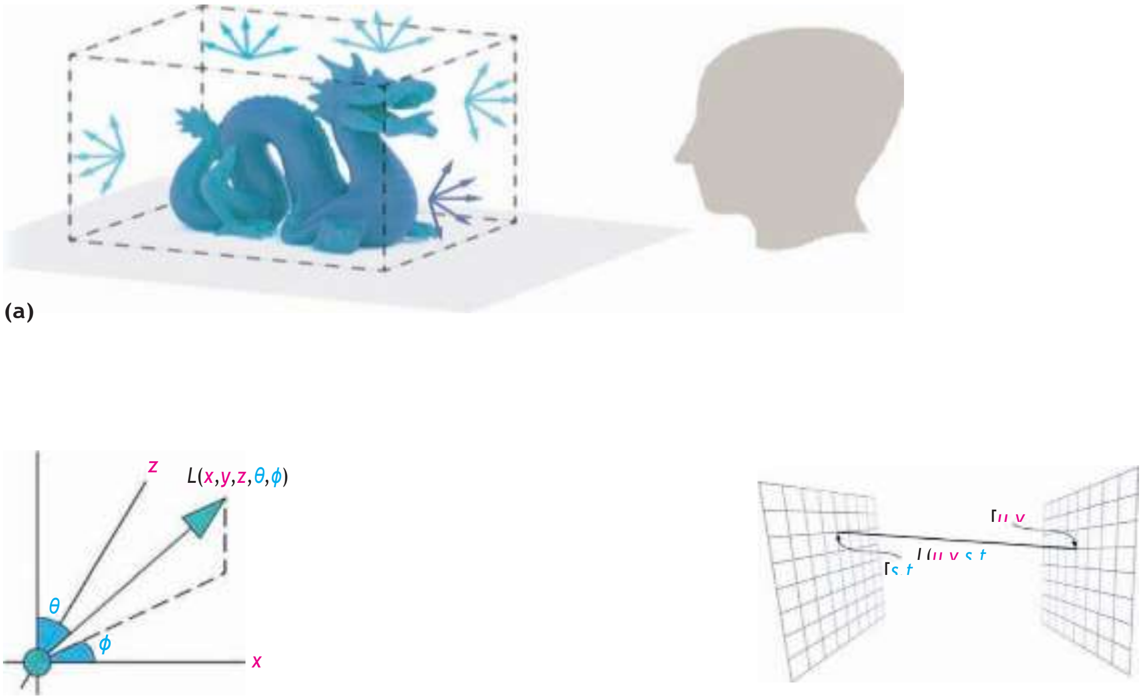

Figure 1.The concept of the light field, (a) which is a vector function that describes the amount of light flowing in every direction through every point in space. The human eye perceives the light field emitting from the surrounding environment. (b) The direction of each ray is given by the 5D plenoptic function, and the magnitude of each ray is given by the radiance. (c) The two- plane parameterization can be used to reduce the plenoptic function to 4D

Understanding Light Fields

The phrase “light field” was first proposed by AndreyGershun in 1936, describing the radiance of light at a certain point given its direction in 3D space.4 More than 50 years later, Edward Adelson and James Bergen proposed using the plenoptic function to represent the light field,5 which encodes the 3D spatial and 2D directional information of a light ray. The plenoptic function is a 5D parametric representation of the light field. Then, in 1996, Marc Levoy and Pat Hanrahan observed that the radiance of a light ray remains unchanged along its propagation direction in free space.6 As a result, they proposed a method to represent the light field using the coordinates of the points at which a light intersects two arbitrary planes. In this manner, the 5D plenoptic function is reduced to 4D, as shown in Figure 1.

The light field records all the spatial information and direction information of the light, so it’s easy to reconstruct images of different focus depths, render images at different viewing angles, and even synthesize an image at a new position. In VR, stereoscopic images or video can be easily constructed from the light-field data, so the resulting stereo image is more realistic than the image produced using traditional binocular-vision reconstruction methods. This is because the traditional binocular-vision syn- thesis of a 3D image is essentially flat, whereas through the light field, the synthesized image is a real 3D image.The development of light-field technology has brought great advances and changes to VR applications. It meets almost all the requirements for VR: stereoscopic parallax can bring people a realistic experience, motion parallax allows people to feel more natural when walking around, and refocusing can make people feel more comfortable with VR content.

Recording Light Fields

The core issue in light-field VR technology is how to record the light-field data and repro- duce the light field for the human eye without any loss of either geometric or photometric information. Light fields can be captured using either a camera array or a light-field camera.Stanford University and the Massachusetts Institute of Technology built multicamera array light-field capture systems, as shown in Figure 2a and 2b. By using a camera array, a high-resolution image can be captured from different viewing perspectives, such that each image corresponds to a 2D slice of the 4D light field. If enough different 2D slices are captured, the 4D light field can be completely reconstructed. The resulting light-field data can be conveniently used to render images from a new perspective, render images at different focus depths, or even increase the resolution and dynamic range of an image or the frame rate of a video.

The other method for obtaining a light field is to use a light-field camera based on a micro- lens array. A light-field camera is a new type of camera, which provides a new refocusing- after-capture feature. The most notable example is Lytro, which has released two models of the light-field camera. Figure 2c is a second- generation light-field camera, Illum. The Ger- man company, Raytrix, provides an alternative light-field camera design, where the micro- lenses have different focal lengths, as shown in Figure 2d.

In essence, the single-lens-based light-field camera samples the angle information through the microlens array. As shown in Figure 3a, each microlens covers a certain number of pix- els. A cone of light from a subaperture of the main lens passes through different positions in each microlens imaging sensor, and this type of position change can be used to obtain directional information about the light. The main lens aperture is divided into numerous sampling units, and each microlens corresponds to the different position of the light field. By put- ting the entire microlens image together, you can obtain the 4D light-field records.

The light-field camera can refocus on any depth plane by rearranging the pixels on the sensor, because it records both position and angle information from the light field. Using Levoy's two-plane light-field parameterization,6 you can render an image at a new focal depth according to the geometric relationships.7 For each 3D point in the scene, you can calculate the coordinates of the points at which the light path intersects with the main lens and the sensor, and the final refocused image can be rendered by integrating the entire corresponding light ray from the light field. Because this virtual refocus plane can be at an arbitrary depth, you can achieve a specific depth of field within any plane by applying this refocusing function.

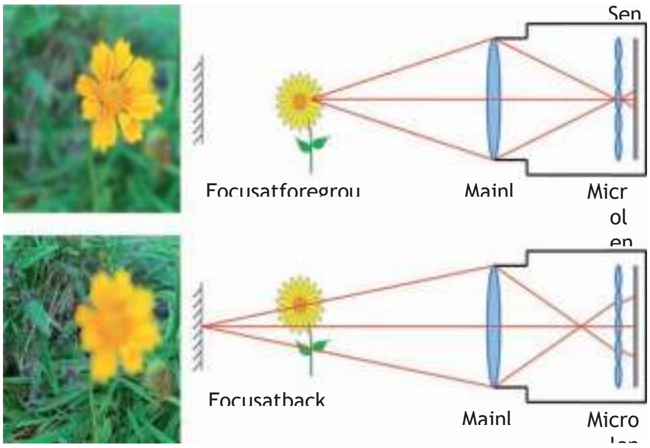

Reference:

[1] B. Wilburn et al., “High Performance ImagingUsing Large Camera Arrays,” ACM Trans. Graphics,vol. 24, no. 3, 2005, pp. 765–776.

[2] Computer Vision and Image Understanding, specialissue on light field for computer vision, April 2016;http://www.sciencedirect.com/science/journal/10773142/145.

[3] A. Gershun, “The Light Field,” J. Mathematics andPhysics, vol. XVIII, MIT, 1939, pp. 51–151.

Institute Vision and Mission

VISION

To be a center of excellence in technical education by using cutting edge technology that produces competent engineers of today and tomorrow to serve the society.

MISSION

- To impart quality education by implementing state-of-the-art teaching-learning methods to enrich the academic competency, credibility and integrity of the students.
- To facilitate a conducive ambience and infrastructure to develop professional skills and nurture innovation in students.
- To inculcate sensitivity towards society, respect for environment and promote high standards of ethics.

Quality Policy

We at Sharad Institute of Technology College of Engineering are committed to provide best quality in planning, design and effective implementation of technical education by involving all stakeholders, upgrading facilities and faculty through continuous improvement.

Shri Shamrao Patil (Yadravkar) Educational & Charitable Trust's

SHARAD INSTITUTE OF TECHNOLOGY, COLLEGE OF ENGINEERING

Yadrav (Ichalkaranji), Dist.-Kolhapur (Maharashtra)

▪ NBA Accredited Programmes ▪ NAAC 'A' Grade Institution ▪ An ISO 9001 : 2015 Certified Institute

AN AUTONOMOUS INSTITUTE

Gat No. 525,473/A Behind Onkareshwar Temple Yadrav-Ichalkaranji, Tal-Shirol, Dist-Kolhapur, Maharashtra, India

Email : contact@sitcoe.org.in, Tel : +91-2322-252796, Fax : +91-2322-252897